Journal of Hydrology 661 (2025) 133533

Contents lists available at ScienceDirect

Journal of Hydrology

journal homepage: www.elsevier.com/locate/jhydrol

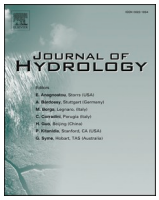

Water-rock interaction processes and hydrogeological pathways in seismically active areas as revealed by a multi-isotopic (C, S, O, H, B, Sr) approach

Lorenzo Chemeri [a,b,*], Marco Taussi [a], Jacopo Cabassi [c,d], Stefania Venturi [b,c,e], Antonio Delgado Huertas [f], Arsenio Granados [f], Samuele Agostini [g], Davide Fronzi [h], Alberto Renzulli [a], Orlando Vaselli [b,c]

[a] Department of Pure and Applied Sciences, University of Urbino Carlo Bo, Via Ca' Le Suore 2/4, 61029 Urbino, Italy
[b] Department of Earth Sciences, University of Florence, Via G. La Pira 4, 50121 Florence, Italy
[c] Institute of Geosciences and Earth Resources (IGG), National Research Council of Italy (CNR), Via G. La Pira 4, 50121 Florence, Italy
[d] Istituto Nazionale di Geofisica e Vulcanologia (INGV), Sezione di Roma1, Via di Vigna Murata 605, 00143 Roma, Italy
[e] Istituto Nazionale di Geofisica e Vulcanologia (INGV), Sezione di Palermo, Via Ugo La Malfa 153, 90146 Palermo, Italy
[f] Laboratorio de Biogeoquímica de Isótopos Estables, Instituto Andaluz de Ciencias de la Tierra IACT (CSIC-UGR), Avda. de las Palmeras, 4, 18100, Armilla, Granada, Spain
[g] Institute of Geosciences and Earth Resources (IGG), National Research Council of Italy (CNR), Via G. Moruzzi 1, 56124 Pisa, Italy
[h] Department of Science and Matter Engineering, Environment and Urban Planning (SIMAU), Marche Polytechnic University, Via Brecce Bianche 12, 60131 Ancona, Italy

ARTICLE INFO

This manuscript was handled by Renato Morbidelli, Editor-in-Chief

Keywords:
Hydrogeochemistry
Stable isotopes
Northern Apennines
Seismically active areas
Water flow

ABSTRACT

Waters circulating in the seismically active (up to 6.4 M_w) Pesaro-Urbino province (central Italy) were investigated to understand water–rock interaction processes and groundwater circulation patterns through a multi-isotopic approach.

The investigated waters showed different geochemical facies: Ca-HCO_3, Ca-SO_4, Ca-HCO_3-SO_4, and Na-HCO_3. Water geochemistry and isotopic composition suggest that Ca-HCO_3 waters are related to the dissolution of carbonate-rich rocks and, subordinately, Al-silicate minerals and are generally characterized by shallow or fast hydrogeological circuits. In contrast, Ca-SO_4, Ca-HCO_3-SO_4, and Na-HCO_3 waters relate to longer water–rock interaction and/or deeper circulation patterns within the aquifers. All the waters show biogenically derived δ^{13}C-TIDC values and δ^{2}H- and δ^{18}O-H_2O signatures indicative of meteoric origin. The combination of δ^{34}S-SO_4 and $^{87}Sr/^{86}Sr$ values suggest that the Ca-HCO_3-SO_4 and Ca-SO_4 waters interact with the evaporitic anhydrite-rich rocks of the Triassic Burano formation that constitute the regional basal aquiclude, making these waters interesting to be monitored for seismic tracers, being likely able to carry possible deep seismic signals (e.g., deep-sourced gases inflow, enhanced metals mobility), similarly to what found in comparable geological contexts. Contrarily, Na-HCO_3 waters show $^{87}Sr/^{86}Sr$ ratios and δ^{11}B values approaching those of the siliciclastic Marnoso Arenacea Fm, consistent with long-lasting interactions with Na-bearing silicates. Our results suggest that the hydrogeochemical and multi-isotopic approach provided paramount information to detect sites more prone to record possible geochemical variations during the build-up phase of seismic events, making it suitable for application to other seismically active areas.

1. Introduction

Water monitoring networks in seismically active areas aimed at the identification of seismic tracers (or precursors), i.e., geochemical and/or isotopic changes that may occur prior to, or concurrently, with a seismic event, are currently developed and deployed worldwide (Barberio et al., 2017; Barberio et al., 2020; Lee et al., 2017, 2021; Hosono et al., 2019; 2020; Hosono and Masaki, 2020; Barbieri et al., 2021; Franchini et al.,

* Corresponding author.
E-mail address: l.chemeri@campus.uniurb.it (L. Chemeri).

https://doi.org/10.1016/j.jhydrol.2025.133533
Received 3 February 2025; Received in revised form 13 May 2025; Accepted 14 May 2025
Available online 17 May 2025

2021; Gori and Barberio, 2022; Chemeri et al., 2024; Chemeri et al., 2025). These geochemical anomalies are generally associated with earthquakes characterized by a magnitude of at least 4 M_w. They may occur from weeks or months before any earthquake or during the event itself (Wang and Manga, 2021 and therein references). Their occurrence indicates that earthquakes (and their preparation processes) can affect groundwater geochemistry and isotopes (e.g., Barberio et al., 2017; Hosono et al., 2020; Franchini et al., 2021; Chemeri et al., 2025). Two main physical mechanisms are generally considered responsible for these variations in groundwaters. The first is related to increased water–rock interaction following the formation of new active (fresh) rock surfaces because of faulting and micro-fracturing (e.g., Claesson et al., 2004; Skelton et al., 2014; Skelton et al., 2019). The second, and more common, is linked to water mixing between two (or more) physically separated aquifers due to changes in the hydraulic head and/or following aquifer breaching triggered by variations in the stress and strain rates during the various seismic stages (e.g., Thomas, 1988; Reddy et al., 2017; Chemeri et al., 2025).

Despite the relevance of the topic, guidelines on how to select the most suitable and sensitive sampling sites (e.g., springs, wells) are not provided, thus making the recognition of seismic tracers challenging. The main difficulties in finding accurate and reliable tracers are (i) the sensitivity of the selected monitoring sites, (ii) the limitation of monitoring periods for producing satisfactory datasets and information, and (iii) the influence of various environmental parameters and possible human errors (Lee et al., 2017, 2021; Franchini et al., 2021). In addition, seismic tracers are site-specific and strictly associated with a given area depending on its geological (i.e., lithology, stratigraphy), hydrogeological (i.e., flow paths, aquifers type) and geodynamic setting (Claesson et al., 2004; Cicerone et al., 2009; Skelton et al., 2014, 2019; Hosono et al., 2019; Hosono et al., 2020; Hosono and Masaki, 2020; Barbieri et al., 2021; Wang and Manga, 2021; Chemeri et al., 2025). Moreover, it must be considered that not all the monitoring sites can detect possible precursory signals of earthquakes and seismic tracers since these sites could be either sensitive or insensitive despite occurring in the same area (Lee et al., 2017, 2021).

A deep understanding of different and simultaneous processes affecting groundwater hydrogeochemistry is a critical step toward selecting the most reliable (and likely sensitive) sampling sites. Water-rock interaction and weathering processes, ion exchange, dissolution, precipitation, and groundwater flow characteristics are the main chemical and physical mechanisms influencing and controlling water chemistry (Deutsch, 2020; Gori et al., 2023). They indeed depend on several hydrogeological factors such as (a) aquifer recharge mechanisms, (b) depth and length of groundwater circulation patterns, (c) type of aquifer systems and related features, (d) occurrence of tectonic features (e.g., fractures or faults) that may favor deep-seated fluids upwelling, and (e) mixing processes between different water types and/or previously separated aquifers (Andreo et al., 2016; Gori et al., 2023 and therein references).

Therefore, the geochemical composition of groundwaters reflects their complex evolution underneath the surface, allowing to reconstruct their flow paths (Doglioni et al., 2014; Smeraglia et al., 2018; Gori et al., 2023). Thus, the hydrologic and hydrogeologic features, together with the lithologies, are fundamental aspects to be considered for establishing a water monitoring network aimed at seismic surveillance. In this context, the application of multiple isotope systematics (C, S, O, H, B, Sr) plays an invaluable and crucial role (Chiodini et al., 2000, 2020; Cortecci et al., 2002; Pawellek et al., 2002; Boschetti et al., 2015; Barbieri et al., 2020; Hosono et al., 2020; Gori et al., 2023; Chemeri et al., 2024; Zhang et al., 2024). Most of these isotopic systems have been proven sensitive to earthquake preparatory phases by changing their original isotopic ratio before or during a seismic crisis (e.g., Boschetti et al., 2019; Skelton et al., 2019, 2024; Barbieri et al., 2020; Hosono et al., 2020; Franchini et al., 2021). Moreover, the isotopic data make it possible to trace the primary sources of some solutes or the secondary processes that affect the waters during their underground circulation, also allowing to identify the geological formations the circulating waters along their paths are interacting with (Clark and Fritz, 1997; Barth et al., 2003; Grassa et al., 2006; Boschetti et al., 2013, 2015, 2019; Bottrell et al., 2019; Vespasiano et al., 2021; Xu et al., 2024). For instance, groundwater circulating through deep aquifers can emerge at the topographic surface as punctual or linear springs after prolonged contact with the host rocks (Tazioli et al., 2024). Therefore, in the case of springs fed by deep fluids, discharging from either highly tectonized areas or well-developed fault systems, their water geochemical and isotopic composition could be functional for recognizing seismic tracers (Lee et al., 2017, 2021; Franchini et al., 2021).

Following a highly detailed geochemical and isotopic characterization of the groundwaters (both springs and wells) located within the seismically active area of the Pesaro-Urbino (hereafter, PU) province carried out by Chemeri et al. (2024), twenty-one sampling sites were selected for further isotopic analyses. These sites were chosen according to (i) geochemical facies, (ii) hydrogeological context, and (iii) location with respect to primary and local seismogenic structures. Beyond the determination of major and trace components, a multi-isotopic approach on each sampling site was carried out by determining oxygen and hydrogen in the water molecule (δ^2H- and δ^{18}O-H_2O), carbon in TDIC (δ^{13}C-TDIC: Total Dissolved Inorganic Carbon), sulfur and oxygen in sulfate (δ^{34}S-SO_4 and δ^{18}O-SO_4), boron (δ^{11}B) and strontium ($^{87}Sr/^{86}Sr$) isotopic ratios in the water phase to (a) define the water–rock (−gas) interaction processes controlling the chemical composition of the selected sites and (b) constrain the origin of the fluids and their possible circulation paths in the shallow crust. By coupling geochemical, isotopic, and hydrological insights, specific sampling sites were considered as the most suitable waters to be included in a monitoring network aimed at defining seismic tracers for the study area, characterized by the presence of seismogenic structures able to generate earthquakes with magnitudes higher than 6 (e.g., DISS Working Group, 2021; Maesano et al., 2023; Pezzo et al., 2023).

2. Overview on stable isotopes application to groundwaters

Stable and radiogenic isotope composition of groundwaters has been proven to be highly effective in interpreting geochemical and hydrogeological processes in natural environments (e.g., Boschetti et al., 2011; Boschetti et al., 2015; Boschetti et al., 2017; Gori et al., 2023; Xu et al., 2024; Zhang et al., 2024). In the present study, hydrogen, oxygen, carbon, sulfur, boron, and strontium isotope systematics were explored to disentangle different information and constraints on the characteristics of the groundwater circulating in the seismically active area of the PU province. Determining water stable isotopes (δ^2H and δ^{18}O) is the most typical application in isotope hydrology since it allows us to define the origin of groundwaters and identify recharge areas (e.g., Nisi et al., 2014). Additionally, many geological processes, some of them also related to the earthquake preparation mechanisms, are often responsible for changes in the relative proportions of the H and O stable isotopes in groundwaters (e.g., Claesson et al., 2004; Claesson et al., 2007). For research purposes, δ^2H and δ^{18}O values provide valuable insights regarding groundwater circulation pathways and allow tracking the possible occurrence of mixing processes between the different aquifers and uprise of deep fluids (Wang et al., 2005; Hosono et al., 2020). The isotopic signature of the total dissolved inorganic carbon (δ^{13}C-TDIC) is widely used in environmental and hydrogeological disciplines to constrain and define the primary source of carbon species (Chiodini et al.,2000, 2020; Barth et al., 2003; North et al., 2003; Grassa et al., 2006; Venturi et al., 2017; Bottrell et al., 2019; Barbieri et al., 2020; Tassi et al., 2022), since each possible end-member is characterized by a specific isotopic range (Cerling et al., 1991; Merritt et al., 1995; Chiodini et al., 2000 and reference therein). The major sources of carbon that contribute to TDIC are represented by (i) dissolution of atmospheric CO_2; (ii) uprise of deep endogenic CO_2 released by mantle degassing

and/or produced as a consequence of the thermal breakdown of limestone under thermometamorphic conditions; (iii) dissolution of carbonate mineral phases (i.e., calcite, dolomite); (iv) inputs and interactions with biogenic CO_2, produced by the oxidation of organic matter trapped into sediments (Cerling et al., 1991; Merritt et al., 1995; Venturi et al., 2017; Tassi et al., 2022). The $\delta^{13}C$ values related to endogenic (and high-temperature) processes in non-volcanic areas generally range from −5 ‰ to + 5 ‰ vs. V-PDB whilst those associated with carbonate dissolution are usually varying between −2 ‰ and + 2 ‰ vs. V-PBD (e.g., Venturi et al., 2017 and references therein). On the contrary, biogenic carbon is preferentially enriched in the lighter isotope, thus showing negative $\delta^{13}C$ values typically below −15 ‰ vs. V-PDB (Merritt et al., 1995; Chiodini et al., 2000; Chiodini et al., 2020). Additionally, the occurrence of secondary processes that may change and alter the original isotopic values needs to be considered (Venturi et al., 2017). In our context, determining the $\delta^{13}C$-TDIC values provides valuable insights into the possible interplay between deep-originated fluids and shallow aquifers.

The application of both $\delta^{34}S$ and $\delta^{18}O$ values in dissolved sulfate (SO_4) allows for the evaluation of sulfur sources and cycles in the aqueous systems and to unravel processes and transformations involving sulfate in the basin catchment (Thode, 1991; Cortecci et al., 2002, 2007; Xu et al., 2024; Zhang et al., 2024). Sulfur may be tangled in multiple processes, determining a wide variability for $\delta^{34}S$ and $\delta^{18}O$. Bacterial reduction of SO_4 is among the main processes that can account for the large variability of sulfur isotopic signatures. Sulfate-reducing bacteria use dissolved SO_4 as an electron acceptor during the oxidation of organic matter, producing H_2S with $\delta^{34}S$ below −20 ‰ vs. V-CDT. On the other hand, $\delta^{34}S$ exceeding + 10 ‰ vs. V-CDT and $\delta^{18}O$ higher than 0 ‰ vs. V-SMOW are usually associated with sedimentary and/or igneous lithologies (MacNamara and Thode, 1950; Holser and Kaplan, 1966; Cortecci et al., 1981; Thode, 1991; Clark and Fritz, 1997; Szaran et al., 1998; Boschetti et al., 2011), thus allowing to identify which geological formation represents the primary source of sulfate (Cortecci et al., 1981; Clark and Fritz, 1997; Cortecci et al., 2002, 2007; Boschetti et al., 2011; Gori et al., 2023 and therein references).

Boron is a ubiquitous constituent in surface and groundwater systems as it mainly derives from rocks and soils weathering containing B-bearing minerals (e.g., Pennisi et al., 2006). The benefit of using boron isotopic content as a geochemical tracer stems from its high mobility at low-to-high temperature fluid-related reactions, matched by significant isotopic fractionation (Leeman and Sisson, 1996). Hence, the application of B isotopes in hydrological investigations marks the origin of dissolved boron and discriminate its sources (Boschetti et al., 2011; Boschetti et al., 2015; Boschetti et al., 2017; Hasenmueller and Criss, 2013; Franchini et al., 2021). The significant mass difference (≈ 10 %) between the two boron stable isotopes ^{11}B and ^{10}B results in a wide range of variation for $\delta^{11}B$ (e.g., Barth, 2000; Pennisi et al., 2006), generally comprised between + 4 and + 58 ‰ vs. NIST SRM 951 for marine B reservoirs and from −31 and + 22 ‰ for non-marine sources, being the isotopic composition of ocean water constant at + 39.5 ‰ (Spivack and Edmond, 1987). Similarly, strontium is mainly present in water systems due to its geochemical affinity with calcium. The $^{87}Sr/^{86}Sr$ ratio is diagnostic of Sr-sources and intimately related to the concentration of Rb; ^{87}Sr is derived by the isotopic decay of ^{87}Rb, while ^{86}Sr is a stable isotope. Thus, the older a Rb-bearing rock is, the higher the $^{87}Sr/^{86}Sr$ ratio. However, when no Rb is hosted in a rock such as limestone, the $^{87}Sr/^{86}Sr$ ratio registers the same water ratio from which the carbonate rock precipitates (e.g., Jørgensen et al., 2008; Nisi et al., 2008; Semhi et al., 2017; Frei et al., 2020). A substantial advantage of the $^{87}Sr/^{86}Sr$ isotopic ratio is that once released into solution, it remains unchanged and reflects the isotopic signature of the original mineral since fractionation processes do not influence it (Bullen et al., 1996), even in waters containing Rb, the ^{87}Rb to ^{87}Sr decay time being of ca. 49 Ga.

3. General background of the Pesaro-Urbino province

3.1. Stratigraphical and tectonic setting

The PU province is located in the northern Marche Region (central-eastern Italy) within the Umbria-Marche Apennines, representing the external part of the Northern Apennines chain that developed during the Miocene. The study area features a variable topography and a complex geological-structural setting (Figs. 1 and 2), with the outcropping geological formations spanning from Lower Jurassic to north-west to Miocene-Pleistocene deposits covered by Quaternary alluvial deposits in the coastal area, to east (Centamore et al., 1971, 1986, 2002; Capuano et al., 1986; Centamore and Micarelli, 1991; Cresta et al., 1989; Barchi et al., 1998a, 2001; Capuano, 2009; Conti et al., 2020; Teloni et al., 2024).

The Umbria-Marche Apennines is an arcuate fold-and-thrust belt, verging towards E-NE, with a major detachment in the Triassic Evaporitic Burano Formation. It is displaced by several thrust fold systems (NNW-SSE) and N-S and E-W oriented strike-slip faults (Barchi et al., 1998a), including the boundary between the Tyrrhenian Umbro-Tuscan extensional area and the Adriatic compressional zone (Meyer et al., 2003).

The Umbria-Marche Apennines are characterized by an average geothermal gradient (~40 mW m^{-2}; Pauselli et al., 2019) and a thick continental crust (Conti et al., 2020 and therein references) composed by an articulated sedimentary succession that started with the deposition of carbonate platform limestones, i.e., Calcare Massiccio Fm (Lower Jurassic) (Fig. 2b). It has to be remarked that the Burano Fm, which is not outcropping in the study area, occurs at the bottom of the succession (Anelli et al., 1994; Capaccioni et al., 2001; Conti et al., 2020), and was reached at 620 and 1550 m depth at the Nerone-Catria and Cesane Ridges areas (Figs. 1 and 2), respectively, during hydrocarbon exploration drillings (Martinis and Pieri, 1964; Barchi et al., 1998b; VIDEPI, 2009). Intra-basinal highs and lows developed following the break-up of the carbonate platform with ongoing carbonate sedimentation represented by micritic pelagic limestones with cherty nodules (Corniola Fm), marly limestones and marls (Rosso Ammonitico, Marne a Posidonia Fm and Bugarone Fm), and then micritic limestones with cherts and calcarenites (Calcari Diasprini Fm). The transition from a predominant carbonate sedimentation towards a marly one is represented by the stratigraphic contact between the Maiolica Fm (mainly limestone and dolomitic limestones) and the Marne a Fucoidi Fm (an alternating marly-to-clay formation) (Capuano et al., 1986; Santantonio, 1993). The uniform marly sedimentation continued through the Cretaceous and Eocene with the deposition of the *Scaglia* Fms, i.e., Scaglia Bianca, Scaglia Rossa, Scaglia Variegata, and Scaglia Cinerea. The deposition of the Bisciaro (marly limestones, marls, and clays with volcanoclastic levels) and the Schlier Fms (marls and clays with locally marly limestones and calcarenites) preceded the turbiditic sedimentation, which began during the Early Miocene (Conti et al., 2020 and reference therein). The siliciclastic succession is represented by the Marnoso Arenacea Fm, consisting of turbiditic sandstones and siltstones interlayered with marlstones (Ricci Lucchi, 1986; Argnani and Ricci Lucchi, 2001; Capuano, 2009), which is overlain by the Tripoli Fm (bituminous clays, marls, sandstones, and diatomites) belonging to the Messinian Evaporitic succession (Tavernelli, 1997; Conti et al., 2020). The coastal area is predominantly composed of silty clays interbedded with sandstones, clays, and evaporites, deposited starting from the Late Miocene to Pleistocene (i.e., Tripoli, Gessoso-Solfifera, San Donato, Colombacci and Argille Azzurre Fms) and overlain by Quaternary alluvial-marine deposits (Nesci et al., 2008; Gallerini and De Donatis, 2009; Taussi et al., 2021).

The PU province represents one of the most seismically active areas in Central Italy and has recently experienced moderate seismicity (Maesano et al., 2023; Pezzo et al., 2023). The area's seismicity is due to two major composite seismogenic sources (DISS Working Group, 2021)

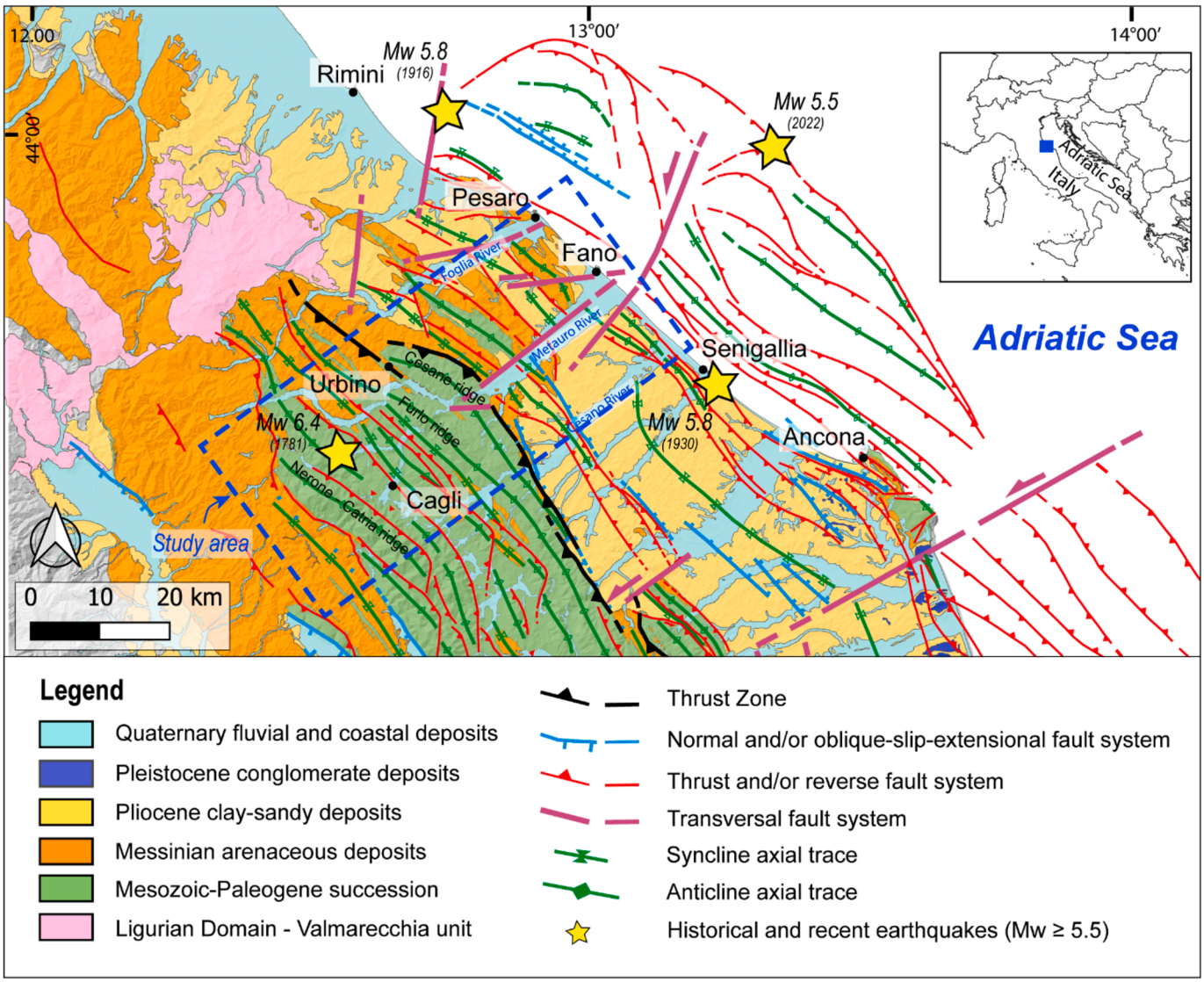

Fig. 1. Structural map of the study area pertaining to the Umbria-Marche Apennines and the offshore area (modified after Teloni et al., 2024 and references therein). The strongest (Mw > 5.5) historical earthquakes that occurred in the area are also reported.

located along the Adriatic coast and offshore areas and the Mt. Catria-Mt. Nerone ridge in the Umbria-Marche Apennines (Fig. 1). The activity on the Adriatic coast and offshore is characterized by events with magnitudes lower than 6 (e.g., the 1916 Rimini – Mw: 5.8 – the 1930 Senigallia – Mw: 5.8 – and the recent Marche offshore – Mw: 5.5 – seismic sequences; Fig. 1) and related with transpressive and compressive structures (Mazzoli et al., 2005, 2014, 2015; Pierantoni et al., 2019; Maesano et al., 2023; Pezzo et al., 2023). Contrarily, along the Apennine chain, the most destructive and strongest events are generally associated with extensional movements (Lavecchia et al., 1994, 2003; Boncio et al., 1998; Boncio et al., 2000; De Donatis et al., 2020) such as the 1781 Cagli earthquake (M_w = 6.4; Fig. 1). However, NW-SE-oriented compressive structures occur in the Cagli area and its surroundings (Mantovani et al., 2014); thus, the presence of such multiple and complex structures makes the identification of the primary source of the events extremely challenging.

3.2. Hydrological and hydrogeological setting

The hydrological framework of the PU province has been revised by Farina and Cavitolo (2016), who, by analyzing 26 rain-gauge stations (from 1980 to 2010) spatially distributed, came out with a mean annual precipitation ranging between 1500 mm/y (in the Apennine ridge) and 700 mm/y (along the coastal areas). The rainiest periods occur in late autumn–winter and spring, while summer is dry. Concerning the thermometric regime, the annual mean temperature in the area varies from 11 °C on the mountain ridge and 15 °C along the Adriatic coast, with lower temperatures in winter and higher temperatures during summer. The water budget calculation performed by Farina and Cavitolo (2016) at an annual scale by applying the Turc method evidences an evapotranspiration pattern ranging between 40 % and 60 % of mean annual precipitation values, moving from the inland to the coastal areas. The hydrogeological characteristics of the PU province are strongly influenced by stratigraphic and tectonic features. The main springs typically emerge near permeability boundaries between different geological formations, and at the contact between lithological contrasts that are reflected in levels or lenses with heterogeneous permeability within the same formation or along significant tectonic lineaments (Boni and Petitta, 2007; Boni, 2010; Mastrorillo and Petitta, 2014; Mammoliti et al., 2023).

From a hydro-stratigraphic point of view (Fig. 2b), the Calcare Massiccio and Corniola Fms and, when present, the Bugarone Fm, host the regional Basal aquifer, which is defined by high infiltration rate and high permeability due to an extensive karstification (Banzato et al.,

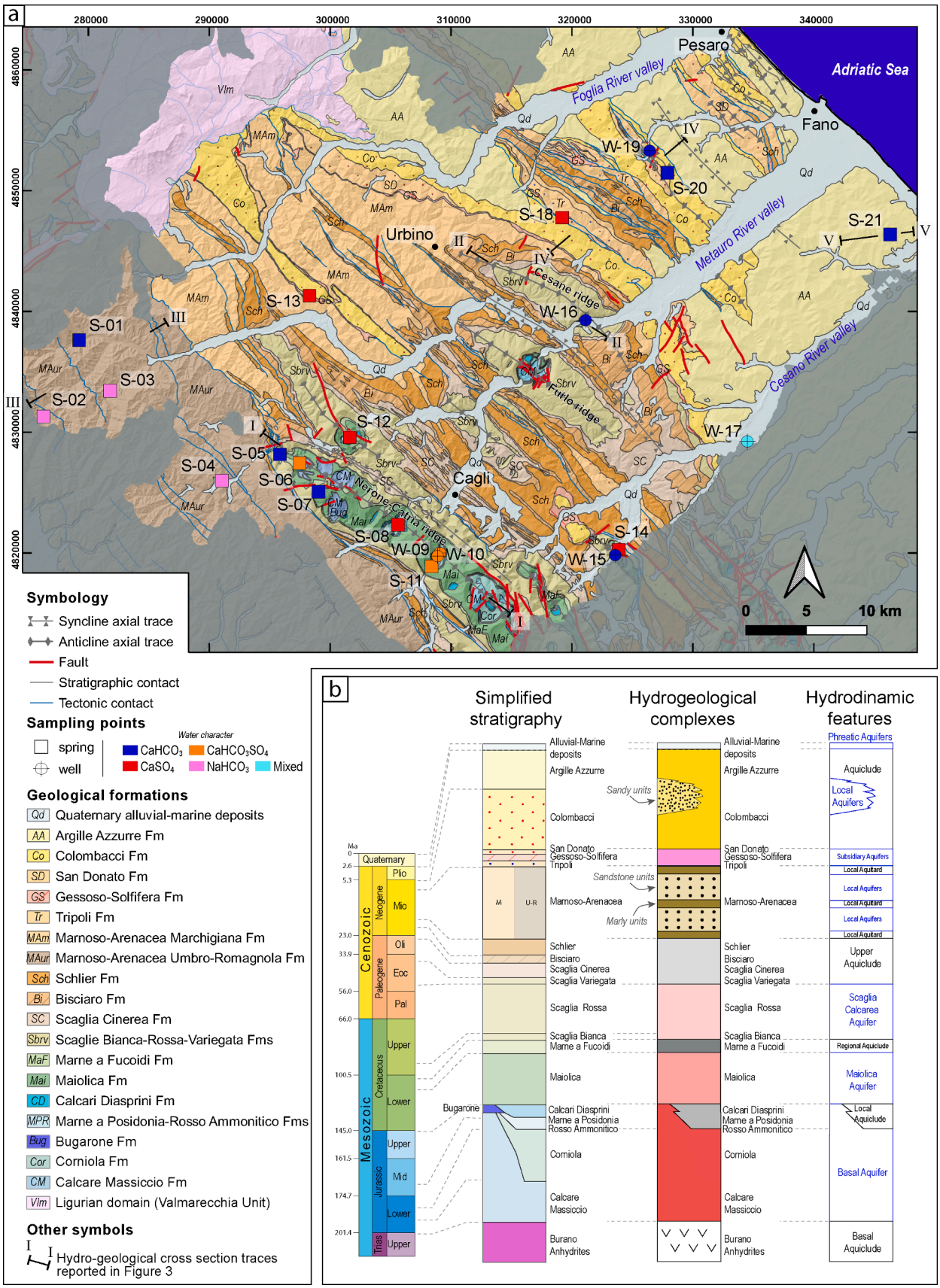

Fig. 2. A) detailed geological map of the study area (after Conti et al., 2020) with the location of the sampling sites and the hydro-geological schematic cross-section traces (Roman numbers) of Fig. 3. The sampling sites are reported according to the emission type (spring or well) and the geochemical character (Chemeri et al., 2024). b) Schematic relationships between stratigraphy (after Conti et al., 2020) and hydrogeological complexes and related hydrodynamic features (modified after Mastrorillo et al., 2009, and Viaroli et al., 2021).

2013; Fronzi et al., 2024a). The Basal aquifer is inferiorly confined by the Triassic Burano Fm, which acts as the regional aquiclude. According to the horst and graben structural setting, formations such as the Rosso Ammonitico, Marne a Posidonia, and Calcari Diasprini are regarded as a localized aquiclude complex, separating the Basal aquifer from the overlying Maiolica aquifer. The Maiolica aquifer is characterized by medium to high permeability due to pervasive stratification and fracture networks (Valigi et al., 2021). At a regional scale, the Basal and the Maiolica aquifers may come into hydraulic contact, constituting a single regional aquifer system. The Maiolica and the Scaglia Calcarea aquifers, the latter located within the Scaglia Bianca and Scaglia Rossa Fms, are separated by the regional Marne a Fucoidi aquiclude. The Scaglia Calcarea aquifer represents the upper aquifer of the carbonate Umbria-Marche domain characterized by medium-to-high permeability due to a well-developed fracture system (Valigi et al., 2020; Fronzi et al., 2022; D'Antonio et al., 2024).

Above the Scaglia Calcarea aquifer, the pre-flysch sequence of Scaglia Variegata, Scaglia Cinerea, Schlier, and Bisciaro Fms closes the calcareous Umbria-Marche sequence, generally acting as an aquiclude. The Early Miocene siliciclastic deposits of the Marnoso Arenacea Fm, as well as the Messinian to Plio-Pleistocene sequence, host local aquifers where the sandstone and sandy-conglomerates prevail (Nanni and Vivalda, 2005). In these geological formations, the local groundwater bodies feed the springs emerging at the contact between more permeable layers or lenses and those displaying lower permeability values composed of marl, silt, and clay layers (Mammoliti et al., 2023). Eventually, the Quaternary deposits, mainly located along the valleys of the rivers and streams, host alluvial aquifers (not covered by this study) that are generally in phreatic conditions (Taussi et al., 2024).

Tectonic features, including folds and faults, exert a significant influence on the groundwater flow (Fig. 3). Faults, depending on their kinematics and activity, may either connect different aquifers (Nanni and Vivalda, 2005; Fronzi et al., 2021; Cambi et al., 2022; Mammoliti et al., 2022) or act as impervious barriers, further shaping groundwater circulation in the study domain. The outcropping areas of the aquifers play an active role in groundwater autogenic recharge (Tamburini and Menichetti, 2020). All aquifers are mainly recharged by precipitation except the alluvial aquifers, in which, in addition to precipitation, recharge from carbonate aquifers may be present (Nanni and Vivalda, 2005). Meteoric recharge in coastal and hilly areas is exclusively due to rainfall, whereas, moving inland towards the carbonate Apennine ridge, snow melting produces a significant recharge to the groundwater systems (Fronzi et al., 2020). Groundwater recharge generally begins in autumn (September-November), when precipitation peaks (usually in November) and air temperature drops, generating an effective excess of water. The recharge continues during winter and spring months, with a second precipitation peak mostly occurring in May. In response to the recharge pattern, the mountain carbonate springs typically reach their maximum discharge value in late spring-summer (April-August). In contrast, springs emerging from local aquifers reach their maximum value in the winter-spring periods (November-May), and some tend to dry up in the summer.

According to the hydro-stratigraphic and tectonic setting (Figs. 2 and 3), as well as the aquifers extension and position across the PU province, numerous springs emerge from the internal carbonate ridges (Fig. 3a,b), where the highest precipitation and recharge rates occur (Farina and Cavitolo, 2016). These springs show high to medium–high flow rates. Springs discharging from the regional Basal aquifer often exceed 300–500 l/s. At the same time, those emerging from the Maiolica and the Scaglia Calcarea aquifers have very variable flow rates as they range from a few L/s to hundreds of L/s (Nanni and Vivalda, 2005). Although the flow rates can significantly vary over the year, the base flow of these springs is always guaranteed due to the considerable extension of the aquifers and the connected fracture system regulating the water movement across the aquifers, making them particularly exploitable for drinking purposes (Capaccioni et al., 2001). Contrarily, the numerous springs emerging from the local aquifers hosted in the Messinian to Plio-Pleistocene geological formations (Fig. 3d,e) have a perennial regime with flow rates of a few liters per second or minute (Nanni and Vivalda, 2005). Carbonate aquifers' geometric and hydrogeological properties typically result in longer water residence times (Aquilanti et al., 2016). However, where the karst system is highly developed, the baseflow sustained by the fracture networks and matrix is supplemented by rapid flow through karst conduits (Nanni et al., 2020). On the contrary, smaller groundwater bodies, hosted in the Upper Pliocene to Pleistocene local aquifers, have shorter and surficial flow paths. The arenaceous and conglomeratic aquifers of the Miocene to Middle Pliocene can instead host water circulating at significant depths and likely interacting with fault systems (Fig. 3c; Nanni and Vivalda, 2005).

4. Materials and methods

4.1. Sampling strategy, in-situ measurements, and geochemical analyses

Twenty-one samples were collected twice from 15 springs and six wells in surveys carried out in February and November 2023, respectively (Fig. 2; Table 1). Water samples were collected based on the results presented by Chemeri et al. (2024) according to (a) their geochemical facies, (b) the location of the sampling sites with respect to regional and local tectonic structures occurring in the study area, (c) the hydro-stratigraphic context and (d) the depth of the wells. According to the hydro-stratigraphic context of the selected sampling sites (Table 1; Fig. 2b, and 3): (a) samples S-06, S-08, W-09, W-10, S-11, S-12, and S-14 are all discharging from the Basal aquifer, W-15 from the Maiolica aquifer and S-05 and S-07 from the Scaglia Calcarea aquifer (Fig. 3a, circulation Type I, afterward); (b) sample W-16 emerges from the Maiolica aquifer (Fig. 3b, circulation Type II, afterward); (c) S-01 to S-04 are discharging from the aquifer hosted in the Marnoso Arenacea Fm (Fig. 3c, circulation Type III, afterward); (d) S-13 and S-18 are emerging from the aquifer interacting with the Gessoso Solfifera Fm, while W-17 from the more permeable layers belonging to the Argille Azzurre Fm (Fig. 3d, circulation Type IV, afterward); (e) W-19 and S-20 emerging from the San Donato and Colombacci Fms, and S-21 discharges from the more permeable layers belonging to the Argille Azzurre Fm (Fig. 3e, circulation Type V, afterward). Concerning the November 2023 survey, data for three samples (i.e., W-17, S-18, and S-19) are unavailable.

Electrical conductivity (EC, in μS/cm at 25 °C), pH, water temperature (T, in °C), and redox potential (Eh, in meV) were measured *in situ* using an *XS PC70 + DHS* multiparametric probe (Table 2). At each sampling site, during the two sampling campaigns, distinct aliquots were collected, as follows: (i) un-filtered aliquot in 125 mL polyethylene (PE) bottles for the analysis of major (HCO_3^-, Cl^-, SO_4^{2-}) and minor (NO_3^-, Br^-, F^-) anions, NH_4^+, SiO_2 and B; (ii) filtered (0.45 μm) and acidified (with 1 % Suprapur HCl) aliquot in 50 mL PE bottles for the analysis of major cations (Ca^{2+}, Mg^{2+}, Na^+, K^+) (Table 2); (iii) filtered (0.45 μm) and acidified (with 1 % Suprapur HNO_3) aliquot in 50 mL PE bottles for trace elements (Li, V, Cr, Mn, Fe, Co, Ni, Cu, Zn, As, Rb, Sr, Ba, Pb; Table S1), and (iv) filtered aliquot in 15 mL plastic tubes for the analysis of water isotopes (δ^2H- and δ^{18}O-H_2O). In February 2023, two aliquots transferred to 12 mL glass vials with a pierceable cap, where $HgCl_2$ was added, were collected to determine the δ^{13}C-TDIC (Total Dissolved Inorganic Carbon). The addition of $HgCl_2$ allows the elimination of microorganisms and organic matter, avoiding any possible fractionation processes after sample collection (Atekwana and Krishnamurthy, 1998). An additional un-filtered 500 mL aliquot was collected in PE bottles for the analyses of δ^{34}S-SO_4 and δ^{18}O-SO_4; for those samples showing negative Eh values, an ammonia-cadmium solution was previously added to separate and remove the sulfur-reduced species ($\sum S^{2-}$) that may be oxidized after sample collection (Montegrossi et al., 2006). Eventually, in November 2023, a filtered 250 mL aliquot was collected in PE bottles to analyze δ^{11}B and $^{87}Sr/^{86}Sr$. Four rock samples, one from the Burano Fm (ALF15; Renzulli et al., 1998) and three from the local

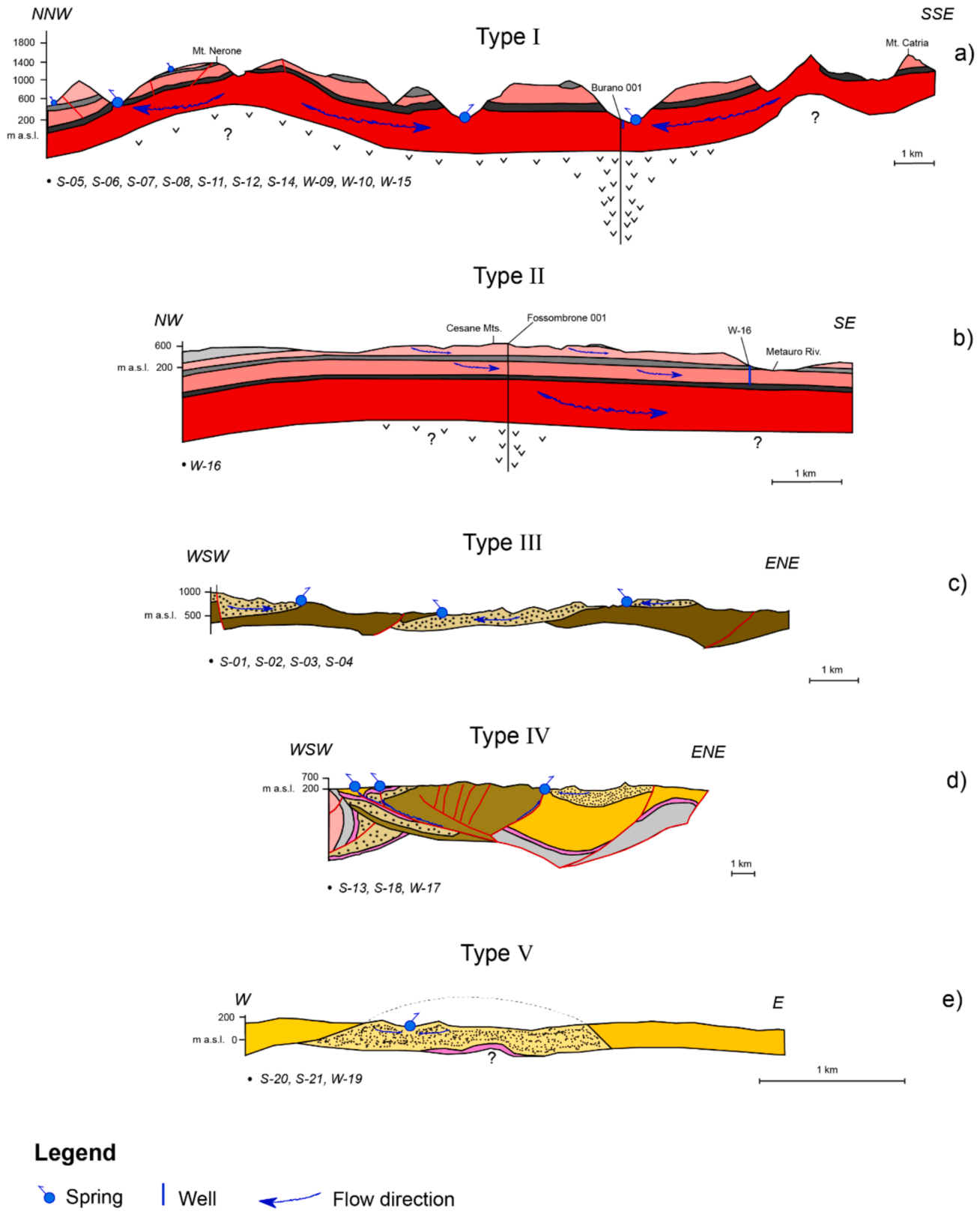

Fig. 3. Simplified hydro-geological models for: (a) carbonate aquifers of Mt. Catria-Mt. Nerone ridge (Type I), modified from Capaccioni et al. (2001); (b) carbonate aquifers of the Cesane Mts. (Type II); (c) terrigenous aquifers hosted in the Marnoso Arenacea Fm., modified after the Carta Geologica d'Italia 1:50,000 Foglio n. 278 "Pieve Santo Stefano" (Type III); (d) terrigenous aquifers hosted in the Miocene to Middle Pliocene Fms (Type IV), modified after Nanni and Vivalda (2005); (e) terrigenous aquifers hosted in the Upper Pliocene to Pleistocene Fms, modified after the Carta Geologica d'Italia 1:50,000 Foglio n. 281 "Senigallia" (Type V). The cross-section traces are indicated with Roman numbers in Fig. 2a, while the colours refer to the hydrogeological complexes' column of Fig. 2b.

Table 1
Samples ID (S: spring, W: well), full name, geographic location (in UTM-33 N WGS84 coordinates), altitude (in m above sea level). The Hydrogeological complexes (referred to Fig. 2b) from which the waters are emerging and the reference hydrogeological circulation types (*H.g. type* referred to Fig. 3) are also indicated.

ID	Full name	Coord_E	Coord_N	Altitude	Lithology of emergence	H.g. type
S-01	Lamoli spring	276267	4831253	748	Marnoso Arenacea	III
S-02	Borgo Pace spring	279237	4837605	373	Marnoso Arenacea	III
S-03	Guinza spring	281792	4833414	528	Marnoso Arenacea	III
S-04	Apecchio spring	291050	4825975	511	Marnoso Arenacea	III
S-05	Sassorotto spring	295852	4828125	411	Scaglia Calcarea	I
S-06	Rio Vitoschio spring	297445	4827418	421	Massiccio Corniola	I
S-07	Monte Nerone spring	299059	4825056	1233	Scaglia Calcarea	I
S-08	Fonte di San Nicolò spring	305585	4822331	344	Massiccio Corniola	I
W-09	Cagli A well	308985	4819931	195	Massiccio Corniola	I
W-10	Cagli B well	308985	4819931	195	Massiccio Corniola	I
S-11	Fontacce spring	308409	4818880	342	Massiccio Corniola	I
S-12	Gorgo a Cerbara spring	301606	4829581	345	Massiccio Corniola	I
S-13	Peglio spring	298292	4841322	462	Gessoso Solfifera	IV
S-14	Bellisio mineral spring	323812	4820247	319	Massiccio Corniola	I
W-15	Cesano well	323709	4819987	321	Maiolica	I
W-16	Fossombone well	321124	4839256	79	Maiolica	II
W-17	San Lorenzo well	334511	4829223	121	Argille Azzurre	IV
S-18	Valzangona mineral spring	319164	4847770	257	Gessoso-Solfifera	IV
W-19	Mombaroccio well	326429	4853303	73	San Donato	V
S-20	Pontaccio spring	327875	4851443	340	Colombacci	V
S-21	Mondolfo spring	346308	4846379	93	Argille Azzurre	V

outcrops of the Gessoso Solfifera Fm (PEG, SBA1, and SBA2) were also analyzed for $\delta^{11}B$ and $^{87}Sr/^{86}Sr$. Prior to the isotopic analyses, the rock samples were cut to remove the presence of possible alteration films. They were then granulated, quartered, and grinded in a planetary mill using agate mortars and spheres.

Total alkalinity was determined by acidimetric titration (AT) within 24–48 h from collection, using an automatic burette filled with 0.01 M HCl and methyl-orange as the colorimetric indicator. Ammonia (NH_4^+) was analyzed using molecular spectrophotometry (MSP) with the Nessler Method using a HACH DR2010 instrument. Major cations and anions were analyzed by ion chromatography (IC), using Metrohm 861 Compact IC and Metrohm 761 Advanced Compact IC chromatographs, respectively. The analytical errors for AT, IC, and MSP were < 5 % (Tassi et al., 2022). The data quality of the main solutes was evaluated by computing the electroneutrality parameter (EP), which was always in the range $\pm$ 5 % (Table 2), thus approaching the electroneutrality principle (Appelo and Postma, 1993).

Trace elements were measured by Inductively Coupled Plasma Mass Spectrometry (ICP-MS) using an Agilent 7800 Mass Spectrometer with an analytical error below 10 %. The accuracy and precision of the analysis were tested using internal and certified international standards, i.e., Aqua 1 e Srls 6 (CNRS-Canada) and DW1 (ISC Science). The chemical compositional analyses were conducted at the Laboratory of Fluid Geochemistry at the Department of Earth Sciences (University of Florence, Italy). Additionally, SiO_2 and B were analyzed at the Gruppo C. S.A. Ltd.'s laboratories (Rimini, Italy) by ICP-AES and ICP-MS, respectively.

4.2. Isotopic analyses

The isotopic analyses of oxygen ($^{18}O/^{16}O$ and expressed as $\delta^{18}O$ ‰ vs. V-SMOW) and hydrogen ($^{2}H/^{1}H$ and expressed as $\delta^{2}H$ ‰ vs. V-SMOW) of waters (Table 3) were carried out using a near-infrared laser analyzer (Picarro L2130-i) using wavelength-scanned cavity ring-down spectroscopy technique (WS-CRDS, analytical errors: $\delta^{18}O \pm 0.08$ ‰, $\delta^{2}H \pm 0.5$ ‰ vs. V-SMOW) (Tassi et al., 2022). The carbon isotopic composition ($\delta^{13}C$-TDIC) was determined following the procedure proposed by Salata et al. (2000): an aliquot of the sample was injected into 12 mL vials that were pre-filled with He and 65 % phosphoric acid (H_3PO_4) and then shaken for 30 s in a Vortex agitator. The vials were left at room temperature for 15–36 h to obtain the equilibrium and separate CO_2. The CO_2 was separated by chromatography in a Gas Bench (Thermo Finnigan) system interfaced with a mass spectrometer. The $\delta^{13}C$-TDIC was then measured using a Delta XP mass spectrometer (IRMS) with an analytical error of $\pm$ 0.1 ‰ (Salata et al., 2000; Verma et al., 2020). The results are reported in ‰ vs. V-PBD (Table 3). The accuracy and precision of the carbon isotopic analyses were validated using three internal standards of Na_2CO_3 solution (DIC-A, DIC-B, and DIC-T), each with a different isotopic composition (-4.90 ‰, -9.50 ‰, $+28.59$ ‰ vs. V-PDB, respectively).

The samples collected for $\delta^{34}S\text{-}SO_4$ and $\delta^{18}O\text{-}SO_4$ analyses were treated as follows: (i) samples with the ammonia-cadmium solution were centrifuged at 3000 rpm for 30 mins to separate the solution from the precipitate (CdS); (ii) a drop of HCl (37 %) was added to the supernatant until a pH < 2 was obtained in order to neutralize the dissolved bicarbonates; (iii) $BaCl_2$ was then added to precipitate $BaSO_4$. The solution was then filtered to separate $BaSO_4$, which was then dried at 50 °C before the isotopic measurement. The sulfur isotopic composition was determined via Delta Plus XL mass spectrometer (EA-IRMS) by combusting the sample with V_2O_5 and O_2 at 1030 °C in a Carlo Erba NC1500 elemental analyzer (Papaslioti et al., 2018). For those samples characterized by low sulfur content, a *purge-and-trap system* was used to allow the collection of 3 μg of sulfur. The analytical error for $\delta^{34}S$ was better than $\pm$ 0.1 ‰; the samples analyzed with the purge and trap system have a precision of $\pm$ 0.3 ‰. The results are reported in ‰ vs. CDT (Canyon Diablo Troilite) (Papaslioti et al., 2018). The $\delta^{18}O\text{-}SO_4$ was determined with a Thermo Finnigan TC-EA high-temperature pyrolysis system coupled to a Delta Plus XL mass spectrometer. The analytical error for $\delta^{18}O\text{-}SO_4$ was $\pm$ 0.3 ‰ vs. V-SMOW (Knöller et al., 2008). Commercial SO_2 was used as an internal standard for sulfur and oxygen isotopes. Besides, different compositions of internal standards with $\delta^{34}S = +23.25$ ‰, $+6.03$ ‰, and -6.38 ‰ (vs. CDT) were prepared and compared with International Atomic Energy Agency (IAEA) standards (Papaslioti et al., 2018). The $\delta^{34}S\text{-}SO_4$ and $\delta^{18}O\text{-}SO_4$ values are reported in Table 3.

Concerning $\delta^{11}B$ analysis, boron was extracted from the water solution following the separation procedure described by Agostini et al. (2021): sample purification was carried out using boron-specific ion-exchange resin (i.e., 20–50 mesh amberlite), loading ca. 0.3–0.4 mL of resin in Savillex PFE Teflon micro-columns, which were previously cleaned with 1.5 N HCl and conditioned with ultrapure high-pH water and ammonia. Water samples were loaded at pH > 10 and rinsed with ultrapure high-pH water and ammonia. In the final step, boron was collected from amberlite using 2 % HNO_3 to prepare a solution ready for

Table 2
Physicochemical parameters and main solutes. The values of pH, temperature (T, in °C), redox potential (Eh, in mV), major anions (CO_3^{2-}, HCO_3^-, F^-, Cl^-, NO_3^-, SO_4^{2-}), and cations (Ca^{2+}, Mg^{2+}, Na^+, K^+ and NH_4^+) and TDS (Total Dissolved Solids), all in mg/L, are reported. bdl = below detection limit. S: spring, W: well. The EP (electroneutrality parameter) for each analysis is also reported.

ID	pH	T	Eh	CO_3^{2-}	HCO_3^-	F^-	Cl^-	Br^-	NO_3^-	SO_4^{2-}	Ca^{2+}	Mg^{2+}	Na^+	K^+	NH_4^+	TDS	EP
S-01																	
F23	6.95	8.5	90	–	342	0.5	16	bdl	2.10	49	105	24	10	1.3	0.01	549	3.50 %
N23	7.42	9.1	120	–	333	0.2	13	0.05	1.28	40	93	23	11	1.6	0.03	515	2.47 %
S-02																	
F23	8.63	14.5	−240	6.5	613	3.1	51	0.46	0.49	11	2	1	277	2.0	0.88	968	0.98 %
N23	9.06	14.1	−255	18.0	635	2.6	61	0.45	0.50	10	9	3	289	1.3	1.85	1032	1.24 %
S-03																	
F23	8.84	14.4	−220	9.5	545	1.3	15	0.08	0.15	13	1	0	223	1.0	0.43	809	−0.87 %
N23	9.37	13.2	−260	33.8	557	1.0	12	0.05	0.20	10	7	1	223	<1.0	0.64	846	−3.11 %
S-04																	
F23	9.15	7.3	−230	22.6	631	3.0	35	0.56	1.72	13	2	1	276	2.8	1.29	990	−0.84 %
N23	9.24	12.6	−175	22.5	640	1.5	40	0.26	0.13	11	10	2	278	1.3	0.86	1008	0.49 %
S-05																	
F23	7.95	10.6	135	–	238	0.0	18	0.06	0.16	4	89	1	7	<1.0	0.01	359	3.62 %
N23	7.98	10.5	110	–	226	0.1	14	0.03	0.15	6	81	1	8	<1.0	bdl	337	3.35 %
S-06																	
F23	7.62	11.3	140	–	218	1.0	14	bdl	2.95	77	89	8	7	1.7	0.01	418	−2.23 %
N23	7.79	11.8	75	–	207	1.0	12	0.03	2.60	248	140	22	7	1.5	bdl	641	0.72 %
S-07																	
F23	7.80	6.6	30	–	179	0.0	11	bdl	1.58	4	66	1	5	1.0	0.08	268	3.99 %
N23	8.11	7.5	135	–	216	0.0	8	0.01	2.35	4	67	1	5	<1.0	0.01	305	−2.87 %
S-08																	
F23	7.28	14.9	175	–	189	3.2	18	bdl	3.30	690	257	65	8	1.7	0.01	1235	0.87 %
N23	7.36	14.2	100	–	180	1.0	19	0.02	1.97	781	297	72	10	2.7	0.01	1364	3.52 %
W-09																	
F23	7.53	9.9	100	–	180	0.3	9	bdl	3.40	143	92	20	4	<1.0	bdl	453	1.73 %
N23	7.77	10	50	–	189	0.4	9	0.03	2.18	143	88	19	5	1.6	0.01	456	−1.74 %
W-10																	
F23	7.65	8.6	−10	–	169	0.3	10	0.07	0.28	227	123	22	5	1.8	bdl	557	2.50 %
N23	7.58	9.9	45	–	174	0.5	9	0.02	2.27	210	117	21	6	2.2	bdl	541	1.96 %
S-11																	
F23	7.63	10.3	215	–	204	0.4	9	bdl	1.26	95	80	13	5	1.0	bdl	408	−3.26 %
N23	7.77	9.3	50	–	194	0.3	8	0.02	2.92	96	89	14	5	0.9	0.05	410	3.29 %
S-12																	
F23	6.86	12.4	−150	–	216	1.3	227	0.66	1.97	819	262	76	168	18.4	0.23	1790	−0.03 %
N23	7–00	12.2	−30	–	210	1.5	266	0.86	1.66	1098	297	97	201	17.3	0.57	2191	−2.84 %
S-13																	
F23	7.25	12.9	50	–	241	1.2	62	bdl	43.95	1378	612	30	42	21.2	0.09	2432	0.24 %
N23	7.45	11.5	10	–	229	2.0	74	0.18	42.50	1451	624	35	56	27.3	bdl	2542	0.41 %
S-14																	
F23	6.96	13.8	−220	–	314	1.2	319	1.85	1.40	544	199	57	247	19.7	1.04	1705	0.63 %
N23	7.06	13.1	−285	–	311	2.4	462	2.14	2.17	727	234	71	319	34.0	2.81	2168	−1.56 %
W-15																	
F23	7.39	13.4	20	–	305	0.3	49	0.22	2.24	64	107	8	33	3.4	0.01	573	−1.47 %
N23	7.23	12.3	90	–	241	0.3	24	0.08	6.33	32	85	5	20	2.8	bdl	415	1,44 %
W-16																	
F23	6.92	13.9	50	–	302	0.5	76	0.34	12.06	26	108	8	43	2.7	0.01	578	0.55 %
N23	7.13	13.5	60	–	317	0.6	173	0.66	3.76	45	102	12	108	3.5	bdl	767	−1.06 %
W-17																	
F23	7.16	16.1	40	–	421	0.2	140	0.75	7.21	72	90	12	174	4.6	0.22	921	2.67 %
N23	–	–	–	–	–	–	–	–	–	–	–	–	–	–	–	–	–
S-18																	
F23	6.52	8.7	−200	–	570	0.7	120	0.31	2.66	1629	587	152	117	10.9	1.43	3190	0.44 %
N23	–	–	–	–	–	–	–	–	–	–	–	–	–	–	–	–	–
W-19																	
F23	6.97	13.4	15	–	616	0.1	65	0.37	13.20	130	164	47	49	2.1	0.04	1087	−2.27 %
N23	–	–	–	–	–	–	–	–	–	–	–	–	–	–	–	–	–
S-20																	
F23	7.09	13.4	45	–	411	0.1	82	0.13	0.88	137	127	48	32	9.9	0.01	847	−0.24 %
N23	6.72	12.7	40	–	418	0.3	65	0.09	0.55	127	126	46	31	9.8	0.01	824	1.23 %
S-21																	
F23	6.94	15	80	–	466	0.3	84	0.39	96.60	125	155	47	65	6.6	0.01	1045	1.36 %
N23	6.81	13.8	30	–	464	0.4	85	0.32	96.56	128	154	46	66	6.7	bdl	1047	1.01 %

ICP-MS analysis after dilution. Boron extraction from the rock samples involved an alkaline fusion step following the procedure described in Agostini et al. (2021). The purified solutions were measured using a Thermo Neptune Plus Multi Collector ICP-MS (MC-ICP-MS). All the samples were diluted to obtain a B concentration of ca. 25 ng/g and bracketed with 25 ng/g NBS 951 boric acid standard solution to reduce the memory effect. The results are reported in ‰ vs. NIST SRM 951 standard with in-run errors in the order of 0.1 ± 0.2 ‰ and external reproducibility within 0.5 ‰ or better (Agostini et al., 2021 and therein references). The analytical procedure for B isotope analysis consisted of sample-reference bracketing using NIST SRM 951 and an on-peak zero blank correction (Guerrot et al., 2011). A triplicate analysis was done for each sample during the same analytical session. The results are given as average delta values without further normalization. The procedural

Table 3
Isotopic composition of the investigated waters: $\delta^{34}S\text{-}SO_4$ (in ‰ vs. V-CDT), $\delta^{18}O\text{-}SO_4$ (in ‰ vs. V-SMOW), $\delta^{11}B$ (in ‰ vs. NIST SRM 951), $^{87}Sr/^{86}Sr$ and $\delta^{18}O\text{-}H_2O$ and $\delta^{2}H\text{-}H_2O$ (both in ‰ vs. V-SMOW), $\delta^{11}B$ and $^{87}Sr/^{86}Sr$ for the rock samples (ALF15, PEG, SBA1 and SB2) are also listed. Results for the B and Sr isotope standards are also reported. S: spring, W: well.

ID	$\delta^{34}S\text{-}SO_4$	$\delta^{18}O\text{-}SO_4$	$\delta^{13}C$-TDIC	$\delta^{11}B$	$^{87}Sr/^{86}Sr$	$\delta^{18}O\text{-}H_2O$	$\delta^{2}H\text{-}H_2O$
S-01							
F23	−14.8	−0.21	−12.37	–	–	−13.80	−78.9
N23	–	–	–	12.6	0.70893	−8.89	−49.8
S-02							
F23	d.n.p.	d.n.p.	−1.67	–	–	−11.67	−65.6
N23	–	–	–	21.3	0.70908	−8.92	−53.5
S-03							
F23	d.n.p.	d.n.p.	−5.95	–	–	−9.56	−61.1
N23	–	–	–	15.9	0.70908	−8.99	−52.2
S-04							
F23	d.n.p.	d.n.p.	−6.11	–	–	−10.76	−60.7
N23	–	–	–	17.2	0.70898	−8.89	−52.1
S-05							
F23	7.85	–	−13.26	–	–	−13.25	−79.0
N23	–	–	–	8.9	0.70781	−8.28	−49.3
S-06							
F23	9.34	9.33	−11.54			−8.11	−47.7
N23	–	–	–	11.3	0.70776	−8.88	−52.0
S-07							
F23	8.38	–	−11.07	–	–	−11.61	−62.0
N23	–	–	–	16.1	0.70762	−9.36	−52.9
S-08							
F23	15.69	15.26	−4.07	–	–	−10.15	−62.4
N23	–	–	–	16.8	0.70768	−9.89	−58.8
W-09							
F23	9.62	11.78	−8.10	–	–	−12.94	−74.2
N23	–	–	–	12.1	0.70770	−9.77	−58.5
W-10							
F23	18.46	12.95	−8.07	–	–	−11.71	−69.8
N23	–	–	–	12.0	0.70769	−9.77	−59.2
S-11							
F23	12.23	10.75	−9.32	–	–	−9.98	−58.7
N23	–	–	–	13.1	0.70772	−9.05	−54.4
S-12							
F23	15.15	8.81	−7.73	–	–	−10.76	−66.8
N23				15.1	0.70769	−8.54	−50.8
S-13							
F23	22.77	12.31	−15.00	–	–	−14.77	−87.2
N23	–	–	–	9.2	0.70892	−8.62	−52.4
S-14							
F23	14.71	8.69	−9.28	–	–	−10.21	−58.8
N23	–	–	–	18.8	0.70769	−7.95	−48.9
W-15							
F23	13.44	9.70	−10.78	–	–	−8.89	−51.8
N23	–	–	–	9.5	0.70776	−8.39	−50.2
W-16							
F23	5.92	9.45	−10.12	–	–	−12.52	−71.0
N23	–	–	–	18.6	0.70762	−9.30	−57.3
W-17							
F23	−13.23	5.62	−12.48	–	–	−11.46	−63.5
N23	–	–	–	–	–	–	–
S-18							
F23	9.99	6.57	−9.10	–	–	−13.08	−72.0
N23	–	–	–	–	–	–	–
W-19							
F23	6.99	6.00	−12.77	–	–	−10.28	−59.3
N23	–	–	–	–	–	–	–
S-20							
F23	6.98	3.15	−10.89	–	–	−9.62	−57.4
N23	–	–	–	25.3	0.70907	−9.09	−53.8
S-21							
F23	9.33	6.26	−12.72	–	–	−8.19	−49.8
N23	–	–	–	27.0	0.70937	−7.58	−45.4
ALF15_rock	14.5*	–	–	8.3	0.70794	–	–
PEG_rock	–	–	–	−3.5	0.70895	–	–
SBA1_rock	–	–	–	−3.4	0.70895	–	–
SBA2_rock	–	–	–	−3.4	0.70894	–	–
IAEA B-5 std	–	–	–	15.14 ± 0.06		–	–
BHVO-2 std	–	–	–		0.703493 ± 0.000007	–	–
AGV-1 std	–	–	–		0.703983 ± 0.000007	–	–

*from Renzulli et al. (1998)

blank and memory effects were corrected, and the sample/blank ratio was generally > 1000. Along with unknown samples, the IAEA B-15 water standard was measured (results are reported in Table 3), as well as five repeated NBS 951 standard processed through complete chemistry with an average of −0.34 ± 0.40 ‰, and four repeated Shelf NBS 951 standard, with an average value of −0.01 ± 0.20 ‰.

Strontium isotopic analyses ($^{87}Sr/^{86}Sr$) were performed using a Thermo Neptune Plus MC-ICP-MS in 2 % HNO_3 solution containing 20–200 ng*g/L of the analyte. Strontium was previously extracted and separated using a Sr-specific resin (Eichrom Sr). Strontium analyses were corrected for mass-bias fractioning with the $^{88}Sr/^{86}Sr$ ratio (=8.375209) and for mass interferences using the ratios of $^{83}Kr/^{84}Kr$ (=0.201750), $^{83}Kr/^{86}Kr$ (=0.664740) and $^{85}Rb/^{86}Rb$ (=2.592310). The rock samples were also analyzed for Sr and B following the same procedure after HNO_3 and HF digestion. The procedural blank and memory effects were corrected, even if the sample/blank ratio was generally > 10,000; thus, the correction was negligible, being inside in-run error values. Along with unknown samples, nine repeated measures of the NBS 987 standard gave an average of 0.710301 ± 0.000004. The results of the samples were adjusted to a value of NBS 987 of 0.710248. Two rock standards (BHVO-2 and AGV-1) were also digested and processed through complete chemistry. The $^{87}Sr/^{86}Sr$ ratios are listed in Table 3.

For more detailed information on B and Sr analytical procedures and data for blanks and standards, we refer to Agostini et al. (2021, 2022), respectively.

The δ^2H- and $\delta^{18}O$-H_2O isotopic analyses were conducted at the Laboratory of Fluid Geochemistry at the Department of Earth Sciences (University of Florence, Italy). The $\delta^{13}C$-TDIC, $\delta^{34}S$-SO_4 and $\delta^{18}O$-SO_4 analyses were performed at the Laboratory of Stable Isotopes Biogeochemistry at the Andalusian Institute of Earth Sciences (IACT) in Granada, Spain. The isotopic analysis of B and Sr were carried out at the Istituto di Geoscienze e Georisorse of the Italian National Research Council (IGG-CNR) in Pisa (Italy).

5. Results

5.1. Water chemistry

The physicochemical parameters and the concentrations of the main solutes are reported in Table 2. The pH values spanned from 6.52 (S-18) to 9.37 (S-03), whereas water temperature (T) was ranging between 6.6 (S-07) and 16.1 (W-17) °C. The redox potential (Eh) varied from −285 (S-14) to +215 (S-11) mV. The Total Dissolved Solids (TDS, intended as the sum of HCO_3^-, Cl^-, SO_4^{2-}, NO_3^-, Br^-, F^-, NH_4^+, SiO_2, Ca^{2+}, Mg^{2+}, Na^+, K^+) showed a wide variability, from 268 (S-07) to 3190 (S-18) mg/L.

Concerning major anions, HCO_3^- was the main component in most of the samples (i.e., S-01, S-02, S-03, S-04, S-05, S-06, S-07, W-09, S-11, W-15, W-16, W-17, W-19, S-20, and S-21), and ranged from 169 (W-10) to 640 (S-04) mg/L. In the water samples with pH > 8.3 (i.e., S-02, S-03, and S-04), CO_3^{2-} varied from 6.5 to 33.8 mg/L. Differently, SO_4^{2-} was the most abundant anion in S-08, W-10, S-12, S-13, S-14, and S-18 with contents up to 1630 mg/L (S-18). Chloride ranged from 8 (S-11) to 462 (S-14) mg/L with high contents (>100 mg/L) also detected in S-12, S-14, W-16, W-17 and S-18. As reported in Table 2, no notable variations in anion abundances were observed between February and November 2023, with the only exception of the S-08 sample that showed a strong increase in SO_4^{2-} from 77 to 248 mg/L, overcoming the bicarbonate content registered in February 2023.

Setting aside S-02, S-02, S-03, S-14, and W-17, where Na^+ showed concentrations up to 320 mg/L, Ca^{2+} was the dominant cation in all the samples, being comprised between 1.4 (S-03) and 624 (S-13) mg/L. High Na^+ contents were also measured at S-12 (168 and 201 mg/L in February and November, respectively), whereas, at W-16, from February to November, Na^+ increased from 48 to 108 mg/L, overcoming Ca^{2+} in November. Magnesium ranged between < 1 (S-03) and 152 (S-18) mg/L, whilst K^+ varied from 0.5 (S-05) to 34 (S-14) mg/L. Following the sample distribution in Fig. 4, the waters can be classified into four major groups: (a) low-to-medium TDS (< 1200 mg/L) calcium-bicarbonate (Ca-HCO_3) waters, including S-01, S-05, S-07, W-15, W-16, W-19, S-20 and S-21; (b) calcium-bicarbonate-sulfate (Ca-HCO_3-SO_4) waters, which are characterized by moderate to strong enrichments in sulfate (up to 250 mg/L) and represented by S-06, W-09, W-10 and S-11; (c) sodium-bicarbonate (Na-HCO_3) waters, also showing alkaline pH values (>8.6) and negative Eh values (< −175 meV), including S-02, S-03 and S-04; and (d) calcium-sulfate (Ca-SO_4) waters, displaying the highest TDS values (i.e., S-08, S-13 and S-18), some of which being characterized by considerable contents in Na^+ and Cl^- (i.e., S-12, S-14) and a Ca(Na)-SO_4(Cl) facies. In addition, the W-17 sample showed a Na(Ca)–HCO_3(Cl) composition. All samples retained the same composition in February and November 2023 apart from W-16, which showed a substantial increase in Na^+ and Cl^- during November and S-08, where the SO_4-component highly increased (Fig. 4).

Among minor elements, NO_3^- was between 0.1 (S-04) and 96.6 (S-21) mg/L, F^- ranged from 0.01 (S-07) to 3.23 (S-08) mg/L, and Br^- from < 0.01 (S-07, S-13) to 2.14 (S-14) mg/L. Eventually, NH_4^+ contents spanned from < 0.01 to 2.81 mg/L (S-14). SiO_2, B, Sr, and other trace element contents are reported in the Supplementary Material (Table S1) and Fig. 5. Dissolved silica (SiO_2) was between 2.5 (W-10) and 35.7 (S-18) mg/L. Boron contents ranged from 8 (S-05) to 5130 (S-14) µg/L, with the higher contents related to the Na-HCO_3 and Ca(Na)-SO_4(Cl) waters, whilst Sr was comprised between 115 (S-03) and 13,500 (S-13) µg/L, with the higher abundances measured in Ca-SO_4 waters. Lithium had concentrations from < 1 and 347 (S-14) µg/L, showing similar behavior to that of B, being enriched in the Na-HCO_3 and Ca(Na)-SO_4(Cl) waters. Manganese, Fe, Zn, and As showed a wide variability (Fig. 5, Table S1). The higher contents were generally related to those samples characterized by high TDS, i.e., peak values were 107 µg/L for Mn (S-18), 314 µg/L for Fe (S-12), 120 µg/L for Zn (S-04) and 17.4 µg/L for As (S-12). Vanadium, Cr, Co, Ni, Cu, and Pb showed very low concentrations in all the samples with no relevant anomaly (Table S1). Rb concentration was below 5 µg/L except for samples S-14 (up to 27 µg/L) and S-12 (up to 21 µg/L). Eventually, Ba ranged from 10 (S-03) to 325 (W-17) µg/L.

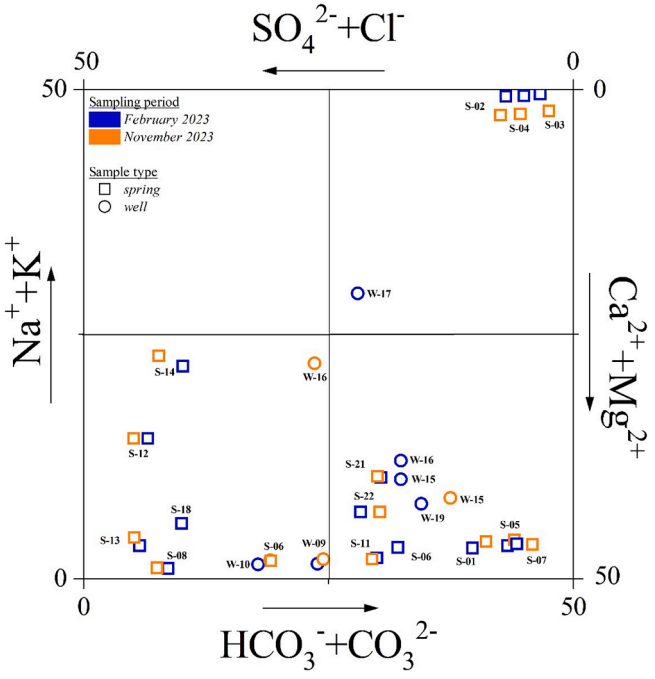

Fig. 4. Langelier and Ludwig (1942) square diagram for the investigated waters. IDs as in Fig. 2a and Table 1.

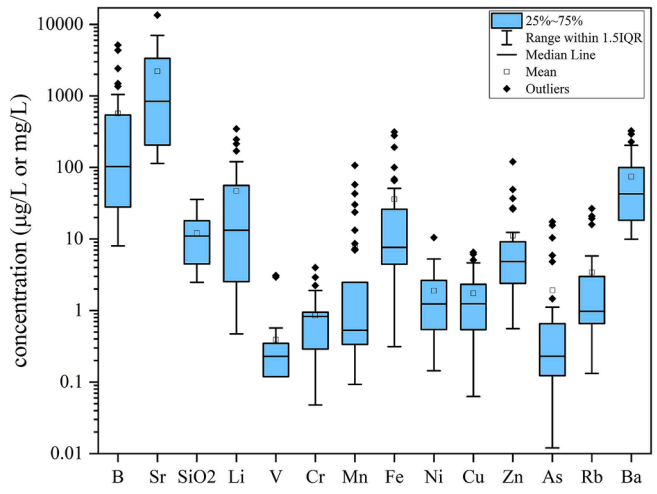

Fig. 5. Box-plots for the trace element contents in the investigated waters. All values are reported in µg/L except for those of SiO_2 that are reported in mg/L. Full results in Table S1.

5.2. Water (and rock) isotopic composition

The complete results of the water isotopic analyses are reported in Table 3. The δ^2H-H_2O values ranged from −87.2 (S-13) and −45.4 (S-21) ‰ vs. V-SMOW, while those of $\delta^{18}O$-H_2O were comprised between −14.8 (S-13) and −7.58 (S-21) ‰ vs. V-SMOW, with all the values measured in February 2023 being significantly lower than those collected in November 2023 (Table 3). The $\delta^{13}C$-TDIC showed relatively negative values, varying between −15.0 (S-13) and −1.67 (S-02) ‰ vs. V-PBD.

The $\delta^{34}S$-SO_4 ranged from −14.80 (S-01) to +22.77 (S-13) ‰ vs. V-CDT, showing all positive values except for S-01 and W-17 (Fig. S1a), thus indicating an enrichment in the heavier isotope (^{34}S). The $\delta^{18}O$-SO_4 values were between −0.21 (S-01) and +15.26 (S-08) vs. ‰ V-SMOW. It is worth mentioning that neither $\delta^{34}S$-SO_4 nor $\delta^{18}O$-SO_4 could be determined in the S-02, S-03, and S-04 samples being characterized by low SO_4 contents, since the amount of precipitate obtained during the sample preparation was not sufficient to perform any isotopic analysis. Moreover, the $BaSO_4$ precipitate obtained for S-05 and S-07 was insufficient for analyzing both sulfur and oxygen isotopes. Therefore, only $\delta^{34}S$-SO_4 was determined (Table 3).

The $\delta^{11}B$ values were all positive and comprised between +8.9 (S-05) and +27.0 (S-21) ‰ vs. NIST SRM 951 (Fig. S1b). Eventually, the $^{87}Sr/^{86}Sr$ isotopic ratio ranged from 0.70762 (S-07) and 0.70937 (S-21). As far as the rock samples are concerned (Table 3), ALF15, representative of the Triassic Evaporitic Burano Fm, showed a $\delta^{11}B$ value of +8.3 ‰ vs. NIST SRM 951 and $^{87}Sr/^{86}Sr$ equal to 0.70794. Contrarily, PEG, SBA1, and SBA2, collected from the Messinian Gessoso Solfifera Fm outcropping near the S-13 water, were characterized by lower values of $\delta^{11}B$ (−3.49, PEG; −3.42, SBA1, −3.44, SBA2, all values in ‰ vs. NIST SRM 951) and higher $^{87}Sr/^{86}Sr$ ratios, i.e., 0.70895 (PEG and SBA1) and 0.70894 (SBA2).

6. Discussion

6.1. Main processes governing water composition

The wide compositional variability of the waters circulating in the PU province can be regarded as the result of multiple water–rock interaction processes acting at different extents (Chemeri et al., 2024) and different hydrological pathways within shallow and deeper aquifers (Fig. 3). The analyzed springs and wells are linked to five hydrogeological reference models (Fig. 3), which serve to clarify the hydrogeological framework in the various investigated areas, with particular focus on potential flow paths within individual aquifers.

The measured δ^2H- and $\delta^{18}O$-H_2O values are reported in Fig. 6, together with the Pesaro-Urbino Meteoric Water Line (PUMWL, Chemeri et al., 2024) and the Central Italy Meteoric Water Line (CIMWL, Longinelli and Selmo, 2003). The samples are distributed following the PUMWL, thus indicating a clear meteoric origin confirming that all the investigated aquifer are recharged by precipitation (Nanni and Vivalda, 2005), with no evidence of ^{18}O-enrichment, since water–rock interactions occurring in low-temperature environments, such as the PU province, do not produce isotope exchange reactions between the infiltrating waters and rock minerals, which are generally ^{18}O-rich (e.g., Capaccioni et al., 2003). Additionally, there is no clustering in the δ^2H and $\delta^{18}O$ values related to the different chemical facies of the samples. The wide variability detected in the groundwater samples (Fig. 6) may be primarily attributable to their spatial distribution (Fig. 2a) since they belong to different topographical contexts characterized by diverse hydrological and hydrogeological conditions (see Section 2.2). For example, S-07 was collected at an altitude of 1233 m a.s.l. while W-19 discharges at 73 m a.s.l., thus implying different recharge areas (e.g., Guan et al., 2009; Minissale and Vaselli, 2011; Hao et al., 2019). Furthermore, these waters circulate within geological and hydrogeological settings characterized by different flow paths (Figs. 2 and 3), which contribute to the observed isotope variability (Fig. 6). This isotopic variability detected between February and November 2023 may be related to seasonal changes (Bowen, 2008; Feng et al., 2012). The air temperatures measured in the 30 days before the February 2023 sampling were significantly lower than those measured before the November 2023 survey, i.e., in the mountain area the average air temperature was 2.4 °C in February 2023 and 13.3 °C in November 2023 (ΔT = 10.9 °C) (data from *Protezione Civile – Regione Marche database*) while in the coastal area, the mean air temperature was 7.1 °C and 18.1 °C (ΔT = 11.0 °C) in February 2023 and November 2023, respectively. As a matter of fact, temperature generally represents one of the main factors influencing the δ^2H- and $\delta^{18}O$-H_2O variability; specifically, lower temperatures favor the enrichment of the lighter isotopes (^1H, ^{16}O), which is consistent with the values measured in the PU groundwaters (Bowen, 2008; Feng et al., 2012; Yang et al., 2019). Furthermore, such changes may be attributable to a different geographic origin of the rainfall events, as observed by Taussi et al. (2024) in the PU coastal area, or more likely to the recharge-discharge mechanisms between different aquifers (Vergni et al., 2016). In fact, the largest carbonate aquifers in

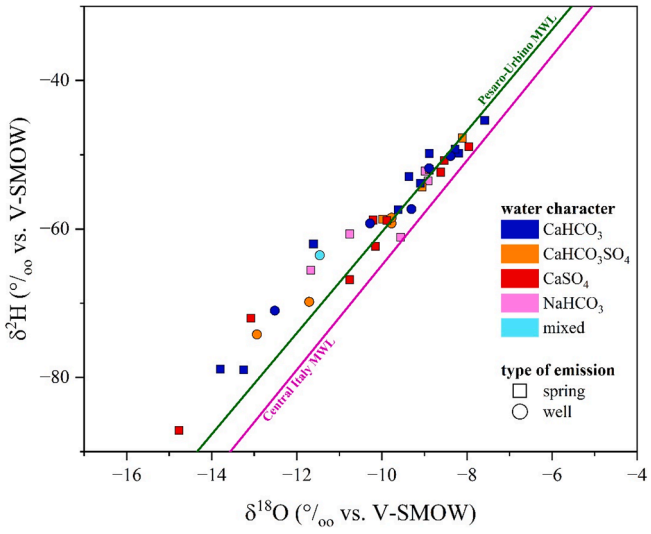

Fig. 6. Binary diagram δ^2H vs. $\delta^{18}O$ (both expressed in ‰ vs. V-SMOW) for the investigated samples, where the Central Italy Meteoric Water Line (CIMWL; Longinelli and Selmo, 2003) and the Pesaro-Urbino Meteoric Water Line (PUWML: Chemeri et al., 2024) are also drawn.

mountain areas often tend to homogenize the meteoric water input, and the fed groundwater systems usually show more constant isotopic values throughout the hydrological year. In this case, the springs generally reflect the mean isotope value of the meteoric waters infiltrating from the recharging areas (Petitta et al., 2010; Fronzi et al., 2021; Tazioli et al., 2024). The water paths in this case are synthesized within the models reported in Fig. 3a, b. On the contrary, aquifers characterized by a minor extension and/or a well-developed karstic system (where the infiltration rate is rapid and comparable to the flow velocity within the groundwater bodies) quickly remove the meteoric waters by evapotranspiration processes. This fact can produce more variable isotopic values during the hydrologic year (reflecting isotopic values of single or cumulative rainfall events). Springs emerging from the Messinian to Plio-Pleistocene aquifers, where effective infiltration only occurs for a few months per year (autumn to winter), usually show an isotopic value that is indicative of meteoric waters exclusively infiltrating during the recharge periods. The spring-to-summer rainwater isotopic values are often not reflected in the groundwater systems (Fronzi et al., 2020; Fronzi et al., 2022). The cycle of these kinds of waters is represented within the models reported in Fig. 3c, d, e.

The Ca-HCO_3 hydrofacies includes most of the waters characterized by low-to-medium TDS values (<1200 mg/L) (Fig. 7a) and does not show any anomaly in terms of pH values and trace element contents. The origin of Ca-HCO_3 waters results by congruent dissolution of carbonate-bearing (i.e., calcite, dolomite) rocks (Fig. 7b, c), in accordance with the geology of the area (Figs. 1 and 2) and consistent with their saturation indexes (Table S2) that approach the saturation values, the latter being also characterized by a higher solubility compared to that of silicate minerals (e.g., Meybeck, 1987). However, slight enrichments in Na^+ may be associated with silicate weathering. Those samples (i.e., S-13 and S-21) showing NO_3 values approaching and exceeding 50 mg/L (i.e., Italian Legislative threshold for water potability) (Table 2) are indicative of anthropogenic activities primarily associated with agricultural practices (Nisi et al., 2022; Taussi et al., 2022), also favored by their shallow hydrogeological circuits (Fig. 3d,e). The compositional shift detected at the W-16 well from February to November 2023, evolving from a Ca-HCO_3 facies towards a Ca(Na)–HCO_3(Cl), can be attributed to a notable decrease of the water table level that is likely favoring the upwelling of deeper (and more saline) fluids. This process is a relatively frequent condition that occurs at the end of the aquifer depletion phase (e.g., Farina et al., 2012).

The S-08, W-09, W-10, and S-11 water samples are characterized by moderate to strong enrichments in SO_4 (up to 240 mg/L), resulting in a Ca-HCO_3(SO_4) character as highlighted in Fig. 4, which reflects the dissolution of gypsum/anhydrite minerals hosted within deeper layers (i.e., Burano Fm) since these waters emerge from carbonate formations linked to the Type I hydrogeological circulation (Fig. 3a) and related to the Basal aquifer (Fig. 2b; Capaccioni et al., 2001; Chemeri et al., 2024). The variable contents in sulfate likely depend on the different degrees of interaction with the anhydrite formations (Capaccioni et al., 2001) or dilution processes with shallower aquifers.

The Ca-SO_4 waters are characterized by the highest values of TDS (up to 3190 mg/L; Fig. 7a). Among this group of waters, the S-08 and S-13 samples have a composition exclusively dominated by Ca^{2+} and SO_4^{2-} with low contents of Na^+ and Cl^- (Table 2), moderate contents of Li and B (Fig. 7c) and no relevant anomaly in metal concentrations (Table S1). On the other hand, the S-12, S-14 and S-18 waters show high values of Cl^- (up to 461 mg/L) (Fig. 7c) and Na^+ (up to 318 mg/L) (Fig. 7b), this latter being predominant compared to Ca^{2+} in S-14 sample. These samples were also showing strong enrichments in B (up to 5000 µg/L), Li (347 µg/L), Rb (up to 27 µg/L), As (up to 18 µg/L), and heavy metals (i.e., Fe, Mn, Zn) (Table S1). Moreover, S-08 and S-13 show positive Eh values (≫+10 mV); contrarily S-12, S-14, and S-18 display strongly negative redox values (≪ −30 mV). The dissolution of $CaSO_4$ hosted by both the Burano Fm and the Gessoso Solfifera Fm represents the most probable origin of these waters (Capaccioni et al., 2001; Chemeri et al.,

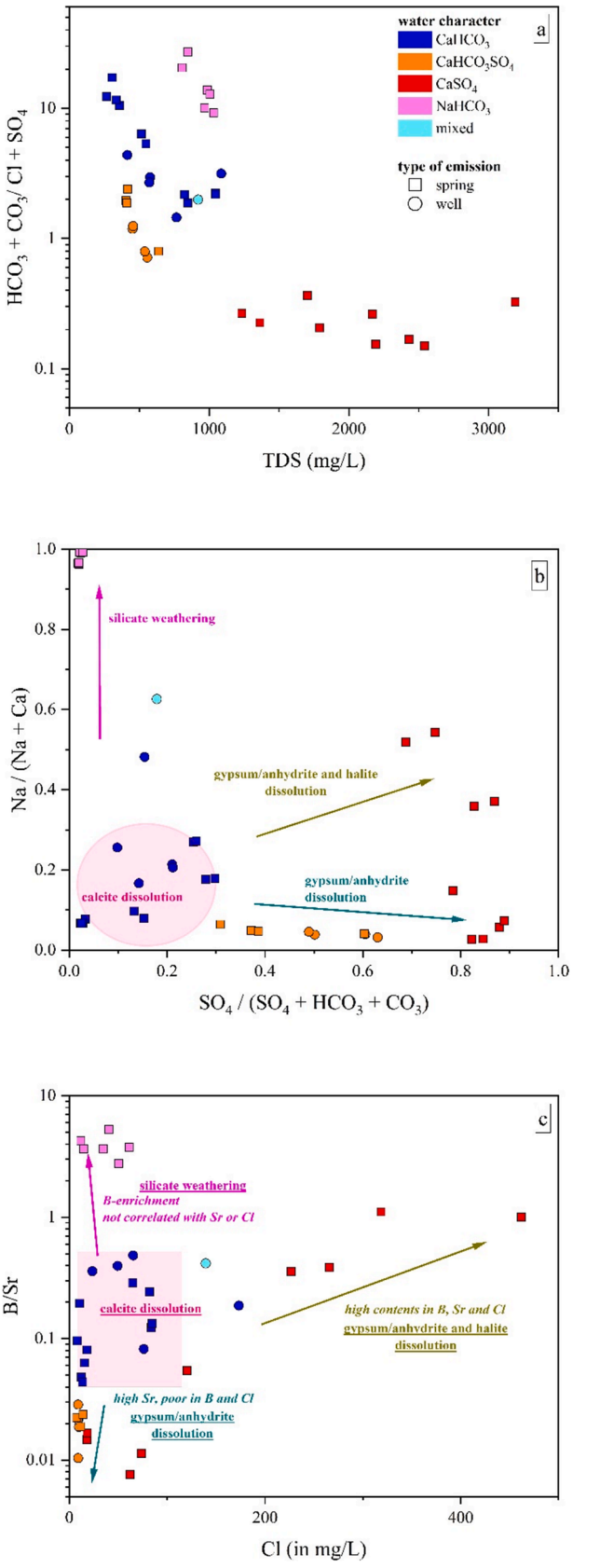

Fig. 7. Binary diagrams of (a) (HCO_3 + CO_3)/(SO_4 + Cl), as molar ratios, vs. TDS (in mg/L), (b) Na/(Na + Ca) vs. SO_4/(SO_4 + HCO_3 + CO_3), as molar ratios, and (c) B/Sr vs. Cl (values in mg/L). In (b) and (c), the most probable processes controlling water composition are also reported according to Frondini (2008) and Chemeri et al. (2024).

2024). The mineral saturation index (Table S2) supports this hypothesis since gypsum (SI_gypsum) and anhydrite (SI_anhydrite) approach the saturation value (SI = 0) (Appelo and Postma, 1993). These evidences suggest that S-08 and S-13 are almost exclusively influenced by the congruent dissolution of gypsum/anhydrite, whilst the high contents of, e.g., Cl^-, Na^+ and B, in S-12, S-14, and S-18 indicate a minor-to-moderate contribution form halite dissolution (Table S2) and silicate weathering, hence producing a Ca(Na)-SO_4(Cl) composition (Fig. 7b,c) (Nanni and Vivalda, 2005; Chemeri et al., 2024). With regards to the hydrogeological circuits and the geographical and geological location of the samples considered (Figs. 2 and 3), it can be preliminarily inferred that S-08, S-12, and S-14 are likely associated with the Burano Fm (circulation Type I), while S-13 and S-18 with the Gessoso-Solfifera Fm (circulation Type IV) (Fig. 3).

The Na-HCO_3 water type, comprising S-02, S-03, and S-04 (Fig. 4), is characterized by high contents in both Na^+ and HCO_3^- species that are not stoichiometrically balanced by Cl^- and Ca^{2+} (and Mg^{2+}), respectively (Table 2). They also show alkaline pH (>8) and negative Eh values, low contents of Sr and Ba, and high concentrations of NH_4, F, Li, and B (Fig. 7b, c) (Venturelli et al., 2000, 2003; Toscani et al., 2001; Chemeri et al., 2024), with B/Cl and Li/Cl ratios higher than those detected in the Ca(Na)-SO_4(Cl) springs, indicating that contributions by Li and B are decoupled from that of Cl^- (Fig. 7c) (Chemeri et al., 2024). These kinds of groundwaters are related to a circulation Type III (Fig. 3c).

The Na-HCO_3 composition is likely acquired by prolonged weathering of Na-rich silicate rocks (Fig. 7c,d), which allows the release of Na^+ in solution, along with B, Li, and F, due to their marked affinity with the former. This hypothesis agrees with the fact that these waters emerge from the siliciclastic Marnoso Arenacea Fm (Figs. 2 and 3), whose interaction with the circulating waters produces alkaline hydrolysis as supported by the high pH values detected in these samples (Venturelli et al., 2000, 2003; Chemeri et al., 2024). The excess in bicarbonate species is likely associated with the $CO_{2(aq)}$ produced by the decay of organic matter trapped into the foredeep sediments, boosted by a reducing environment (negative Eh values) that facilitates silicate weathering (Cortecci et al., 1999; Toscani et al., 2001; Venturelli et al., 2003; Vespasiano et al., 2023; Chemeri et al., 2024).

The W-17 sample is characterized by a predominant Na-HCO_3 composition but not comparable to the S-02, S-03, and S-04 waters since it shows higher contents of Cl^-, SO_4^{2-} and Ca^{2+} (Fig. 4). Therefore, its composition may be the result of multiple processes acting at different extents like silicate weathering and gypsum and halite dissolution enhanced by the presence of faults that favor the connection between the aquifers hosted in the Gessoso-Solfifera Fm and the Plio-Pleistocene silicate deposits, relating to circulation Types IV and V (Fig. 3d; Nanni and Vivalda, 2005).

6.2. Isotopic constraints on water–rock interaction processes and hydrological circuits

6.2.1. Total dissolved inorganic carbon isotopic composition (δ^{13}C-TDIC)

The investigated waters are characterized by δ^{13}C-TDIC values < -1.67 ‰ vs. V-PDB with less negative δ^{13}C values associated with the Na-HCO_3 and Ca(Na)-SO_4(Cl) waters (Table 3; Fig. 8a). These values are consistent with the dissolution of calcite and the interaction with biogenic soil CO_2 as the primary sources for the origin dissolved carbon species (Fig. 8b) (e.g., Grassa et al., 2006; Bottrell et al., 2019).

In the Na-HCO_3 waters, the pH becomes the predominant factor influencing the resulting δ^{13}C-TIDC values (Fig. 8b). In fact, under alkaline pH values (>8.6), during the interaction processes between dissolved $CO_{2(gas)}$ and bicarbonate $HCO_{3(acq)}$, the heavier isotope (^{13}C) is preferentially enriched in the aqueous solution (Clark, 2015; Bottrell et al., 2019). This condition would explain the less negative values detected in S-02 (−1.67 ‰ vs. V-PDB), S-03 (−5.95 ‰ vs. V-PDB), and S-04 (−6.11 ‰ vs. V-PDB). The δ^{13}C-TIDC values are consistent with those

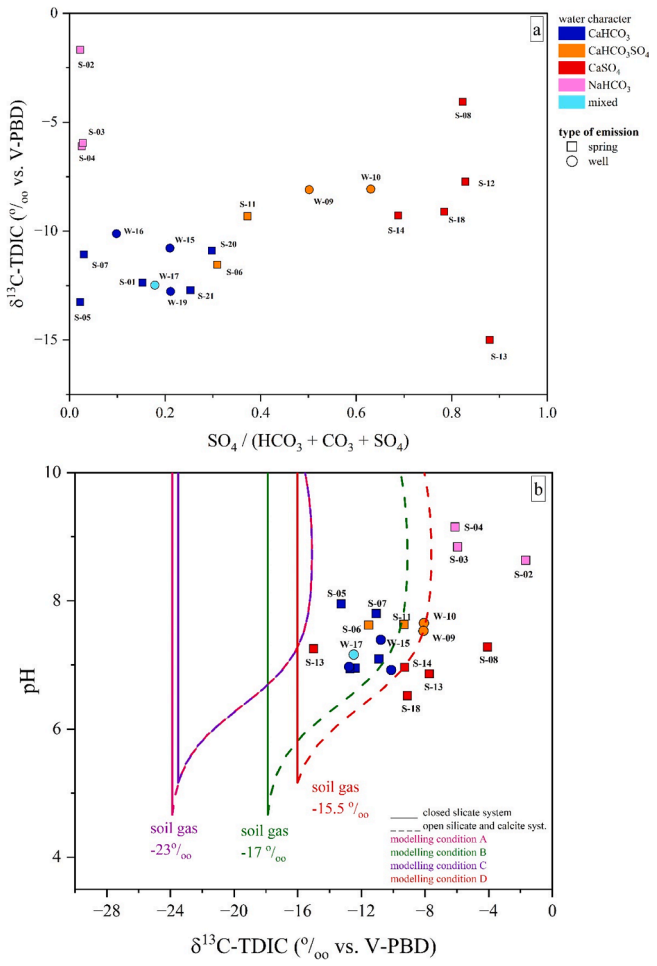

Fig. 8. Binary diagram of (a) δ^{13}C-TDIC (in ‰ vs. V-PBD) vs. $SO_4/(HCO_3 + CO_3 + SO_4)$ (as molar ratios) and, (b) pH vs. δ^{13}C-TDIC (in ‰ vs. V-PBD). Evolution lines describing the δ^{13}C-TDIC values at different pH values are also reported, under four modelling conditions according to Bottrell et al. (2019), considering infiltrating waters at different pCO_2 in equilibrium and interacting with soil CO_2 with multiple δ^{13}C signatures in closed silicate system and open silicate and calcite system, respectively. Full details on the modelling conditions and equations are described in Bottrell et al. (2019). IDs as in Fig. 2a and Table 1.

of δ^{13}C-CO_2 and δ^{13}C-CH_4, reported by Chemeri et al. (2024), indicating a predominant biogenic origin for carbonate species produced at relatively shallow depths (with a minor influence from limestone dissolution) (Fig. 3c), with absent or negligible contributions from deep-seated fluids.

6.2.2. δ^{34}S and δ^{18}O of dissolved sulfate

The use of sulfur and oxygen isotope systematics in the PU waters is of notable importance since some of them (i.e., S-06, S-08, W-09, W-10, S-11, S-12, S-13, S-14, and S-18) are characterized by either a Ca-SO_4 composition or a strong sulfate enrichment (Fig. 4). In both cases, sulfate can be derived by the interaction with the anhydrite-bearing Triassic Burano (TBf) or the gypsum-bearing Messinian Gessoso Solfifera (MGf) Fms (Figs. 2 and 3), which lie at the bottom and the top of the Umbro-Marche succession, respectively (Fig. 2b) (Conti et al., 2020 and therein references). Thus, if the chemical contribution of SO_4^{2-} is isotopically different, it is possible to define and constrain the hydrological circuits (Fig. 3). Indeed, the δ^{34}S- and δ^{18}O-SO_4 values from TBf and MGf are characterized by different isotopic ranges (Fig. 9), with some overlaps only related to the δ^{18}O-SO_4 isotopic ratios. Specifically, the TBf values of δ^{34}S-SO_4 range between +12 and +19 ‰ vs. V-CDT while those

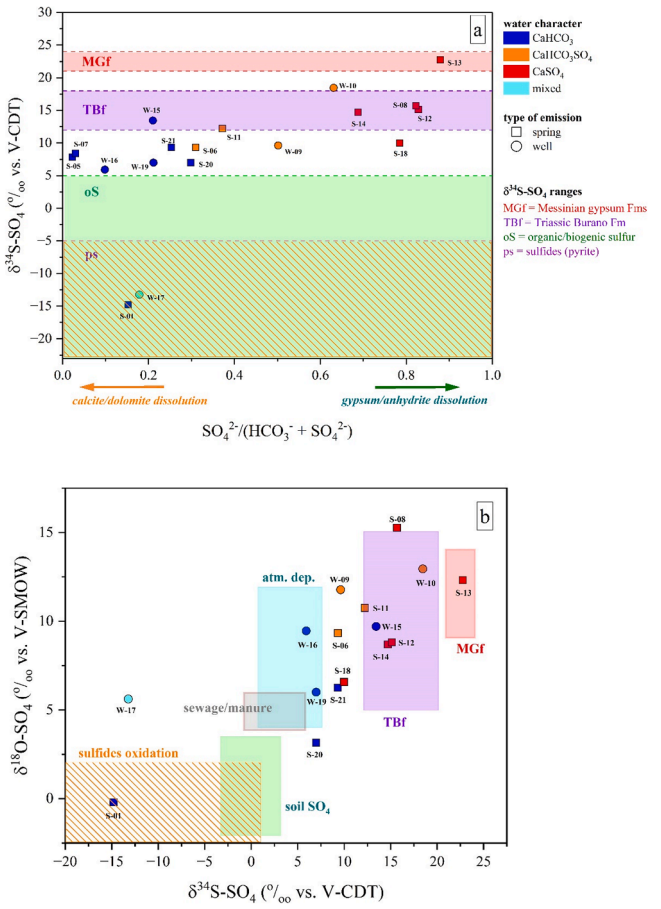

Fig. 9. Binary diagrams of (a) δ^{34}S-SO$_4$ (in ‰ vs. V-CDT) vs. SO$_4$/(SO$_4$ + HCO$_3$) in molar ratio, and (b) δ^{18}O-SO$_4$ (in ‰ vs. V-SMOW) vs. δ^{34}S-SO$_4$ (in ‰ vs. V-CDT). The isotopic ranges for different sulfate sources are reported for comparison to Cortecci et al. (1981), Clark and Fritz (1997), Pawellek et al. (2002), Menichetti et al., (2017) and Gori et al., (2023). Acronyms are: TBf (Triassic Burano Fm), MGf (Messian gypsum Gessoso Solfifera Fm), oS (organic/biogenic sulfur) and ps (sulfides − pyrite). IDs as in Fig. 2a and Table 1.

of δ^{18}O-SO$_4$ are between +5 and +15 ‰ vs. V-SMOW (Cortecci et al., 1981; Renzulli et al., 1998; Pawellek et al., 2002; Boschetti et al., 2011; Menichetti et al., 2017). Contrarily, MGf has δ^{34}S-SO$_4$ values ranging from +21 to +24 ‰ vs. V-CDT, and those of δ^{18}O-SO$_4$ are within +8 and +14 ‰ vs. V-SMOW (Clark and Fritz, 1997; Lugli et al., 2007; Gori et al., 2023).

In the PU waters, the more positive δ^{34}S values (>+10 ‰ vs. V-CDT) are usually associated with those waters where the gypsum-anhydrite dissolution is predominant compared to that of carbonate-bearing minerals (SO$_4$ ≫ HCO$_3$ + CO$_3$) (Fig. 9a). The samples' δ^{34}S- and δ^{18}O-SO$_4$ are reported in Fig. 9b. As expected, according to the geographic location and the geological-hydrogeological context of the sampling sites (Figs. 2 and 3), the S-13 water discharges from a hill where the Gessoso Solfifera Fm is largely outcropping (Tamburini et al., 2017), and falls within the *MGf* field, pointing that the sole source of sulfate is related to the Messinian gypsum. Contrarily, the other SO$_4$-rich water samples (i.e., S-06, S-08, W-09, W-10, S-11, S-12, S-14, and S-18) and the Ca-HCO$_3$ W-15 sample (located close to S-14) are discharged from the Basal aquifer (Fig. 3a) with their sulfate isotopic values falling close, or within, the *TBf* field, indicating a likely interaction with the Burano Fm. Nevertheless, the influence of secondary processes, like *microbially-mediated* sulfate reduction, cannot be ruled out, at least for those waters (e.g., S-12, S-14) characterized by strongly negative Eh values (<-30 meV). Among the SO$_4$-rich water samples, the location of S-18 (Fig. 3d) contrasts with the SO$_4$ isotopic signature. This spring is located far from the carbonate anticline (Fig. 2a), where the TBf have been identified at > 1500 m depth in a deep well (Martinis and Pieri, 1964; Barchi et al., 1998b; VIDEPI, 2009; Fig. 3b), thus suggesting that the interaction with TBf is unlikely. On the contrary, the lighter δ^{34}S-SO$_4$ value of S-18 could be influenced by mixing processes with reduced and isotopically negative sulfur, as recognized in the bituminous shales characterizing the MGf (e.g., Lugli et al., 2007).

The Ca-HCO$_3$ waters, i.e., S-05, S-07, W-16, W-19, S-20, and S-21 (no δ^{18}O-SO$_4$ values are available for the first two samples), tend to be positioned between or within the *TBf*, *atmospheric deposition* and *soil SO$_4$* fields, therefore suggesting a mixed origin. Based on the lithology from which these waters are discharged, they can be associated with shallow hydrogeological circulation (Table 1; Fig. 3). The S-05, S-07, and W-16 waters are discharged from the Maiolica and Scaglia Calcarea aquifers separated from the Basal aquifer by regional aquicludes (see Section 2.2; Table 1 and Fig. 2b) and show low SO$_4$ concentrations (< 45 mg/L; Table 2). These characteristics make unlikely a TBf influence on the δ^{34}S-SO$_4$ values, at least for the S-07 and W-16 samples. On the contrary, S-05, despite having SO$_4$ concentrations < 10 mg/L, occurs near a well-developed normal fault (De Donatis et al., 2020) that might facilitate deep circulation. The W-19, S-20, and S-21 waters show relatively high levels of SO$_4$ (120–140 mg/L), but shallow hydrogeological circuits are envisaged (Fig. 3d,e) in areas characterized by intense agricultural activity (Taussi et al., 2024). In these cases, sulfate seems thus more likely sourced by anthropogenic activities related to manure fertilizers or sewage (Puig et al., 2017). Eventually, the S-01 and W-17 samples are discharged by arenaceous and clay formations (Marnoso Arenacea Fm and Argille Azzurre Fm, respectively) that may contain sulfides (Conti et al., 2020 and reference therein), whose oxidation produces SO$_4$ preferentially enriched in ^{32}S (Cortecci et al., 2002; Gori et al., 2023), resulting in light or negative δ^{34}S- and δ^{18}O-SO$_4$ values (Fig. 9b).

6.2.3. Boron and strontium isotopes

The binary diagram of the δ^{11}B values vs. the boron content (in µg/L) for the investigated waters is reported in Fig. 10a. For comparison are also reported the isotopic ranges for the most likely source of dissolved B (i.e., limestones, marine evaporites, clays, and seawater) (Barth, 1993, 2000; Dotsika et al., 2010; Boschetti et al., 2011, 2015, 2017, 2019) and the samples (i) ALF15 (δ^{11}B = +8.3 ‰ vs. NIST SRM 951, *purple line*), and (ii) PEG, SBA1 and SBA2 (δ^{11}B = −3.4 ‰ vs. NIST SRM 951, *red line*), representative of the local TBf and MGf, respectively. The δ^{11}B values of the local rocks are lower than those generally found in marine evaporites (i.e., +18 ‰ < δ^{11}B < +32 ‰ vs. NIST SRM 951; Barth, 1993; Boschetti et al., 2019), hence showing a moderate-to-strong ^{11}B-depletion, especially for the MGf. Owing to the wide isotopic variability of boron (e.g., Barth, 1993), the presence of overlapping ranges does not allow us to distinguish a single source of B since all the samples are included within the limestone, clay, and marine evaporite fields (Fig. 10a). On one hand, this may represent a limit when only the boron isotopes are determined in an environment characterized by a relatively high variability as that observed for the PU waters. On the other hand, this may indicate the occurrence of multiple sources that define the B isotopic composition involving carbonates, evaporites, and silicate minerals interaction with waters, which were recognized as the main processes controlling the water composition.

Additional constraints can be highlighted by the Sr isotopes (Fig. 10b). The ^{87}Sr/^{86}Sr ratios measured in the local MGf rocks (0.70894–0.70895; Table 3) agree with those reported in the literature for the Umbria-Marche-Romagna MGf (e.g., Berrettoni et al., 1986; Lundblad, 2019; Franchini et al., 2021). Contrarily, the local TBf value (0.70794; Table 3) is slightly higher but consistent with those reported by Lundblad (2019) for the Umbria-Marche TBf (0.70776 and 0.70778) (Fig. 10b). Concerning the investigated waters, two groups of samples can be identified according to their ^{87}Sr/^{86}Sr ratios: (i) ^{87}Sr/^{86}Sr ranging from 0.70762 and 0.70781 (S-05, S-06, S-07, S-08, W-09, W-10, S-11, S-12, S-14, W-15, W-16) and falling within the TBf and limestones (i.e.,

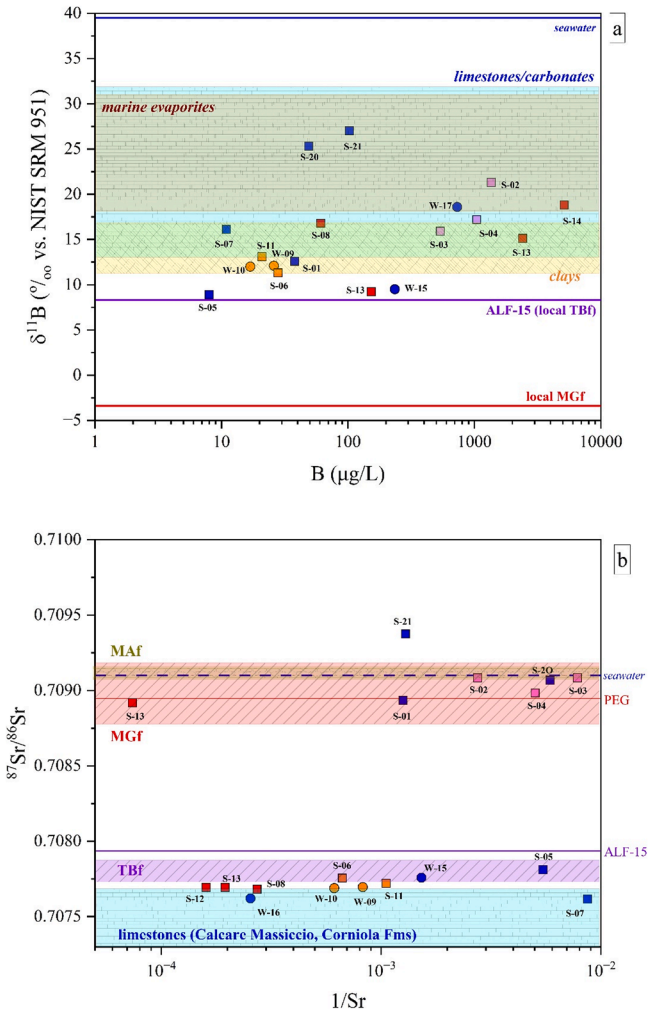

Fig. 10. (a) $\delta^{11}B$ (in ‰ vs. NIST SRM 951) vs. B content (in µg/L). Isotopic ranges for the most probable B sources in the study area (i.e., limestones, marine evaporates and clays) are drawn according to Barth (1993) and Boschetti et al. (2019). (b) $^{87}Sr/^{86}Sr$ vs. 1/Sr (values in mg/L). Isotopic ranges for the outcropping geological formations (i.e., limestones, Marnoso Arenacea Fm, Triassic Burano Fm TBf and Messinian Gessoso Solfifera Fm MGf) in the study area are also reported following Berrettoni et al. (1986), Castorina and Masi (2011) and Lundblad (2019). The $\delta^{11}B$ and $^{87}Sr/^{86}Sr$ values measured for the local rocks, i.e., ALF-15 (TBf, violet line) and PEG (MGs, red line), and seawater are also reported. Symbols as in Fig. 5; IDs as in Fig. 2a and Table 1.

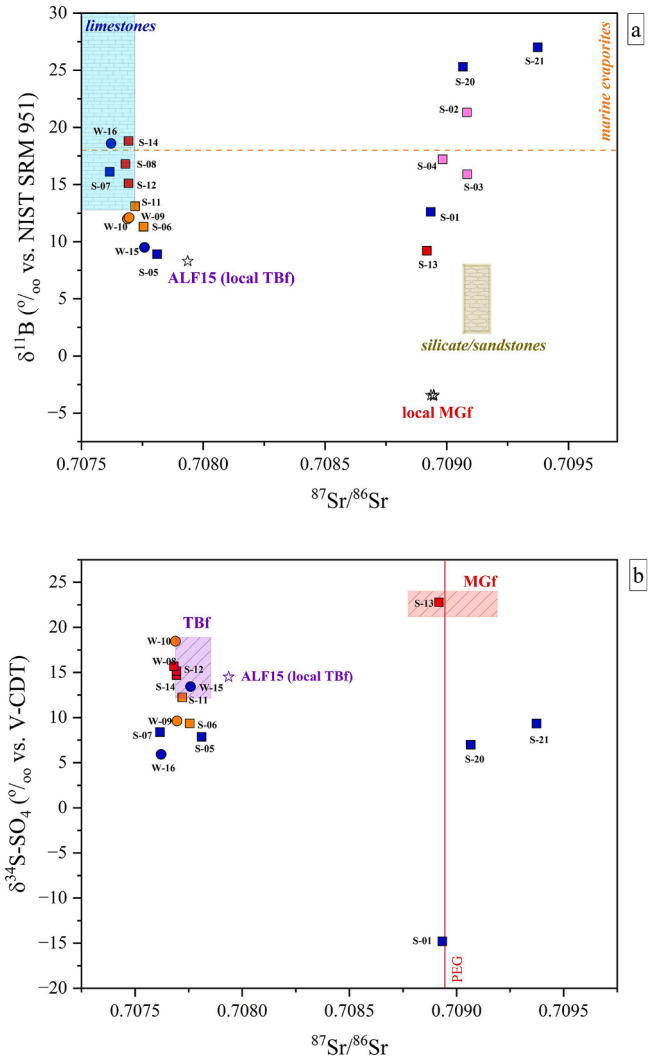

Fig. 11. (a) $\delta^{11}B$ (in ‰ vs. NIST SRM 951) vs. $^{87}Sr/^{86}Sr$. Isotopic ranges for both B and Sr in limestones and siliciclastic sediments/sandstones are reported after Barth (1993), Castorina and Masi (2011), Boschetti et al. (2019) and Lundblad (2019). The $\delta^{11}B$ range, commonly related to marine evaporites, is also reported (Barth, 1993). Stars indicate the $\delta^{11}B$ and $^{87}Sr/^{86}Sr$ values measured in the local rocks TBf (Triassic Burano formation: ALF15) and MGf (Messinian Gessoso Solfifera formation: PEG, SBA1 and SBA2). (b) $\delta^{34}S\text{-}SO_4$ (in ‰ vs. V-CDT) vs. $^{87}Sr/^{86}Sr$. The isotopic ranges for TBf and MGf are reported after Berrettoni et al. (1986), Renzulli et al. (1998); Menichetti et al. (2017) and Lundblad (2019). The star refers to the ALF15 sample ($\delta^{34}S\text{-}SO_4$ from Renzulli et al., 1998), while the vertical line refers to the $^{87}Sr/^{86}Sr$ ratios measured in the PEG sample. Symbols as in Fig. 5; IDs as in Fig. 2a and Table 1.

Calcare Massiccio and Corniola Fms) isotopic ranges (Lundblad, 2019); (ii) $^{87}Sr/^{86}Sr$ ratios included between 0.70892 and 0.70937 (S-01, S-02, S-03, S-04, S-13, S-20, S-21), approaching the reference values of MGf and the carbonate fraction of the Marnoso Arenacea Fm (Berrettoni et al., 1986; Castorina and Masi, 2011).

The distribution of the first group of samples in Fig. 10b suggests that the primary source of Sr (and consequently of Ca) is represented by TBf and/or limestones, which is consistent with the main geochemical processes occurring in these waters (Fig. 7b, c) and with the hydrogeological features of the areas where they circulate (Figs. 2 and 3), i.e., the Basal aquifer (Fig. 2b). The dual contribution from these lithologies is evident when the Sr and B ratios are considered together (Fig. 11a) since all the samples (i.e., S-05, S-06, S-07, S-08, W-09, W-10, S-11, S-12, S-14, W-15, and W-16) depict a well-defined trend between the limestone end-member (Barth, 1993; Boschetti et al., 2019; Lundblad, 2019) and the local TBf, whose input can also be inferred by coupling $\delta^{34}S\text{-}SO_4$ and Sr isotopes since all the abovementioned samples fall within or close the *TBf* field (Fig. 11b).

Among the aforementioned samples, S-07 and W-16 fall within the limestone field (Fig. 11a), showing a null contribution from TBf, as suggested by their hydrogeological circuits (Figs. 2 and 3, Table 1). On the contrary, samples S-05, S-06, S-08, W-09, W-10, S-11, S-12, S-14, and W-15 show various degrees of inputs from the TBf since they circulate in the Basal aquifer (Figs. 2 and 3, Table 1).

The dissolution of TBf is predominant in the S-08, S-12, and S-14 samples (which also show SO_4-dominated compositional facies) and in the Ca-HCO_3-SO_4 waters (i.e., S-06, W-09, W-10, S-11) and acts at a smaller extent for the S-05 and W-15 samples (i.e., Ca-HCO_3 waters), where limestone/carbonate dissolution is prevailing (Fig. 7b, c). On the contrary, the second group of waters (S-01, S-02, S-03, S-04, S-13, S-20, S-21) has $^{87}Sr/^{86}Sr$ ratios suggesting that MGf and the Marnoso Arenacea are the most likely Sr-sources (Berrettoni et al., 1986; Castorina and Masi, 2011). The S-02, S-03, and S-04 samples are characterized by Na-

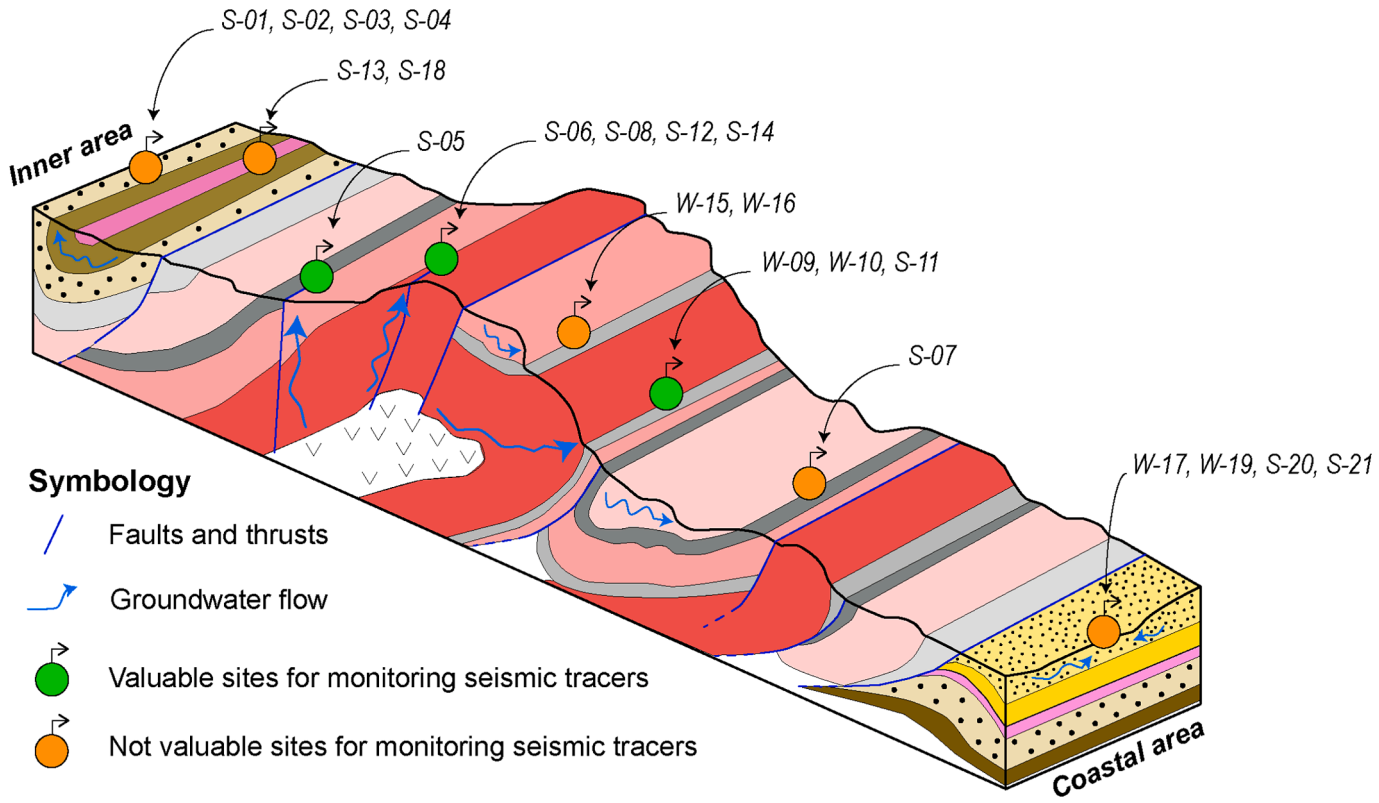

Fig. 12. Conceptual model summarizing the hydrogeological circuits of the investigated sites, which helps to define the most valuable setting to be monitored for possible seismic tracers' recognition in the investigated area of the Pesaro-Urbino Province. The sketch follows and modifies the schematic model of Nanni and Vivalda (2005). Colours refer to the hydrogeological complexes' column of Fig. 2b.

HCO_3 compositional facies (Fig. 4), a substantial depletion in Sr and Ca (Fig. 7c; SM1), and $^{87}Sr/^{86}Sr$ values approaching that of the Marnoso Arenacea Fm from which they emerge after a long-lasting interaction in a shallow and slow hydrogeological circuit (Fig. 3c). The S-01 sample (Ca-HCO_3 water) circulates in the same geological context as S-02, S-03, and S-04 (Fig. 2a). Hence, even if the $^{87}Sr/^{86}Sr$ ratio is very similar to that of the local MGf, considering its chemical composition and hydrogeological circuit (Fig. 3c) a Sr contribution from the Messinian evaporites is to be excluded. At the same time, that from the Marnoso Arenacea Fm appears realistic. On the other hand, MGf represents the predominant source of Sr (and Ca) in the S-13 sample, having virtually the same $^{87}Sr/^{86}Sr$ ratio (Fig. 11b), which is also consistent with the surrounding geology (Fig. 2a) and its chemical composition (Ca-SO_4).

Eventually, S-20 and S-21 samples are characterized by $^{87}Sr/^{86}Sr$ ratios of 0.70907 and 0.70937 (Table 3), respectively, approaching the value measured in PEG which may suggest MGf as the primary source of Sr. Contributions deriving from MGf may be consistent with the local hydrogeology (Figs. 2 and 3d,e) and with the relatively high SO_4 contents (up to 137 mg/L). However, the $\delta^{34}S$-SO_4 values of S-21 (+9.33 ‰ vs. V-CDT) and S-20 (+6.98 ‰ vs. V-CDT) are consistent with an anthropogenic source (see Section 5.2.2), hence making MGf a possible minor source of both dissolved strontium and sulfur.

7. Conceptual model and concluding remarks

The application of a geochemical and multi-isotopic (i.e., C, H, O, S, Sr, and B) approach to groundwaters from seismically active areas, characterized by a wide geological and hydrogeological variability like the Pesaro-Urbino province, is a powerful tool to constrain water–rock interactions and provide insights into the hydrological paths. In deploying a water geochemical monitoring network to identify possible seismic tracers, selecting the most suitable sampling sites, i.e., those related to longer circulation paths and fed by deep aquifers (circulation Types I and II in Fig. 3a, b), is a fundamental and necessary step. A conceptual model of the main hydrogeological, geochemical, and isotopic findings of the present work are summarized in Fig. 12.

The groundwaters circulating in the study area are characterized by four main geochemical facies: Ca-HCO_3, Ca-HCO_3-SO_4, Ca-SO_4, and Na-HCO_3 compositions. The carbon isotopic data ($\delta^{13}C$-TDIC) hint at a limited or negligible influence of deep-originated fluids in the shallow environment with the primary carbon sources represented by either the dissolution of carbonate-bearing minerals or the interaction with biogenic soil CO_2. The combined application of $\delta^{34}S$-SO_4 and $^{87}Sr/^{86}Sr$ allowed the identification of a group of waters represented by Ca-HCO_3-SO_4 (i.e., S-06, W-09, W-10, and S-11) and Ca-SO_4 (S-08, S-12, and S-14), which interact with the Triassic Burano Fm (TBf) (Fig. 3a and 12). Since TBf is not outcropping since it was found at a minimum depth of 600 m below the surface, the isotopic evidence suggests that these waters may be subjected to circulation patterns able to reach deep levels, with their emergence at the surface likely favored by the presence of faults (Fig. 12). Boron isotopes also support this evidence since these waters displayed $\delta^{11}B$ values consistent with mixing between the local TBf and limestones (the lithology from which these waters emerge). Contrarily, the S-13 sample, although showing a Ca-SO_4 composition, is related to circulation within the Gessoso Solfifera Fm (MGf) as supported by Sr, S, and B isotopic values and the local hydrogeological context (Fig. 3d and 12).

The Na-HCO_3 waters (i.e., S-02, S-03, and S-04) showed $^{87}Sr/^{86}Sr$ like those of the Marnoso Arenacea Fm and $\delta^{11}B$ values approaching the reference values for siliciclastic sediments and sandstones. These ratios are consistent with the hypothesis that the origin of these waters is related to long-lasting interactions with Na-bearing silicate minerals in a shallow hydrogeological circuit (Fig. 3c and 12). Water geochemistry and isotopic contents suggest that the Ca-HCO_3 waters are likely related

to shallower or faster water circulation, interacting with limestones and silicate-rich rocks widely outcropping in the study area.

In conclusion, our results suggest that (most of) the Ca-SO_4 and Ca-HCO_3-SO_4 waters are discharged by the Basal aquifer after long and deep flow paths that lead to water–rock interactions with the local deep-seated TBf (Fig. 12), maintaining the isotopic signature of the primary source (almost) unchanged and thus less affected by secondary processes; notably, faults can play a critical role in facilitating groundwater circulation from deep layers to the surface (Fig. 12), especially during seismic periods, when they can act as preferential flow features. Indeed, these kinds of water have been widely found to be sensitive to possible geochemical and isotopic variations in similar geological-tectonic contexts such as the Sibillini Mts. (Marche Region) or the Gran Sasso Mt. area (Abruzzo Region) (e.g., Barberio et al., 2017; Barbieri et al., 2020; Fronzi et al., 2021; Cambi et al., 2022). For these reasons, these springs and wells can be considered as the most valuable sites for monitoring seismic tracers (Fig. 12), being likely able to carry possible deep seismic signals. Although further information on the circulation path of the deep-related waters could benefit from tritium analysis and continuous or periodical acquisition of specific parameters (e.g., EC, T, discharge rate), the multi-chemical and isotopic approach carried out in this study was proven to be effective to select the most prone sites likely able to record possible geochemical variations during the build-up phase of a seismic event. The results of this work make our approach applicable to other geological contexts where seismic activity is well-documented, thus taking a step further to mitigate the seismic hazard.

CRediT authorship contribution statement

Lorenzo Chemeri: Writing – review & editing, Writing – original draft, Visualization, Validation, Methodology, Investigation, Formal analysis, Data curation, Conceptualization. **Marco Taussi:** Writing – review & editing, Visualization, Validation, Supervision, Methodology, Investigation, Conceptualization. **Jacopo Cabassi:** Writing – review & editing, Validation, Investigation, Formal analysis, Conceptualization. **Stefania Venturi:** Writing – review & editing, Visualization, Investigation. **Antonio Delgado Huertas:** Writing – review & editing, Formal analysis. **Arsenio Granados:** Writing – review & editing, Investigation. **Samuele Agostini:** Writing – review & editing, Formal analysis. **Davide Fronzi:** Writing – review & editing, Writing – original draft, Validation, Investigation, Visualization. **Alberto Renzulli:** Writing – review & editing, Supervision, Resources, Conceptualization. **Orlando Vaselli:** Writing – review & editing, Supervision, Resources, Investigation.

Declaration of competing interest

The authors declare that they have no known competing financial interests or personal relationships that could have appeared to influence the work reported in this paper.

Acknowledgements

The authors wish to thank Dr. Francesco Capecchiacci and Dr. Chiara Macelli for their help and assistance in the analytical analyses at the Department of Earth Sciences of University of Florence; Dr. Paolo Di Giuseppe for the support during sample preparation and analyses at the IGG-CNR in Pisa; Dr. Hector Díaz-Alejo, Dr. Paul Rosero and Dr. Nerea Ruiz for the help in sample preparation at the Andalusian Institute of Earth Sciences in Granada. Dr. Martina Casalini and Dr. Federica Meloni (University of Florence) are kindly thanked for their hints provided while writing the discussion. During the development of the study, LC was financially supported by a ReMeST PhD Grant (XXXVII cycle) financed by the University of Urbino. MT was financially supported by a research contract co-financed by the European Union "ESF-REACT-EU, PON Research and Innovation 2014–2020 D.M. 1062/2021 (grant n. 63-G-19603–1)". Three anonymous reviewers, former Editor C. Corradini and Editor R. Morbidelli are sincerely thanked for their valuable comments that helped to improve a previous version of our work.

Appendix A. Supplementary data

Supplementary data to this article can be found online at https://doi.org/10.1016/j.jhydrol.2025.133533.

Data availability

Data used in this work are presented in the text and in the supplementary material.

References

Agostini, S., Di Giuseppe, P., Manetti, P., Doglioni, C., Conticelli, S., 2021. A heterogeneous subcontinental mantle under the African-Arabian Plate boundary revealed by boron and radiogenic isotopes. Sci. Rep. 11, 11230. https://doi.org/10.1038/s41598-021-90275-7.

Agostini, S., Di Giuseppe, P., Manetti, P., Savascin, M.Y., Conticelli, S., 2022. Geochemical and isotopic (Sr-Nd-Pb) signature of crustal contamination in Na-alkali basaltic magmas of South-East Turkey. It. Journal of Geosc., 141 (3), 363–384. https://doi.org/10.3301/IJG.2022.21.

Andreo, B., Gil-Márquez, J.M., Mudarra, M., Linares, L., Carrasco, F., 2016. Hypothesis on the hydrogeological context of the wetland areas and springs related to evaporitic karst aquifers (Malaga, Cordoba and Jaén provinces, southern Spain). Environ. Earth Sci., 75 (9), 1–19. https://doi.org/10.1007/s12665-016-5545-1.

Anelli, L., Gorza, M., Pieri, M., Riva, M., 1994. Subsurface well data in the northern Apennines (Italy). Mem. Soc. Geol. It., 48, 461–471.

Aquilanti, L., Clementi, F., Nanni, T., Palpacelli, S., Tazioli, A., Vivalda, P.M., 2016. DNA and fluorescein tracer tests to study the recharge, groundwater flowpath and hydraulic contact of aquifers in the Umbria-Marche limestone ridge (central Apennines, Italy). Environ. Earth Sci. 75, 1–17. https://doi.org/10.1007/s12665-016-5436-5.

Argnani, A., Ricci Lucchi, F., 2001. Tertiary silicoclastic turbidite systems of the Northern Apennines. In: Vai, G.B., Martini, I.P. (Eds.), Anatomy of an Orogen: the Apennines and Adjacent Mediterranean Basins. Kluwer Academic Publishers, Dordrecht, pp. 327–350.

Appelo, C., Postma, D., 1993. Geochemistry, groundwater and pollution. Balkema, Rotterdam, Netherlands.

Atekwana, E.A., Krishnamurthy, R.V., 1998. Seasonal variations of dissolved inorganic carbon and δ13C of surface waters: application of a modified gas evolution technique. J. Hydrol., 205, 265–278. https://doi.org/10.1016/S0022-1694(98)00080-8.

Banzato, F., Mastrorillo, L., Nanni, T., Palpacelli, S., Petitta, M., Vivalda, P.M., 2013. L'acquifero Carbonatico Fratturato Delle Sorgenti Del Fiume Aso (parco Nazionale Dei Monti Sibillini): Valutazioni Sulla Risorsa Rinnovabile e Sull'area Di Alimentazione. Frabosa Soprana, Italy.

Barberio, M.D., Barbieri, M., Billi, A., Doglioni, C., Petitta, M., 2017. Hydrogeochemical changes before and during the 2016 Amatrice-Norcia seismic sequence (central Italy). Sci. Rep. 7 (1), 11735. https://doi.org/10.1038/s41598-017-11990-8.

Barberio, M.D., Gori, F., Barbieri, M., Billi, A., Caracausi, A., De Luca, G., Franchini, S., Petitta, M., Doglioni, C., 2020. New observations in Central Italy of groundwater responses to worldwide seismicity. Sci. Rep. 10, 17850. https://doi.org/10.1038/s41598-020-74991-0.

Barbieri, M., Boschetti, T., Barberio, M.D., Billi, A., Franchini, S., Iacumin, P., Selmo, E., Petitta, M., 2020. Tracing deep fluid source contribution to groundwater in an active seismic area (central Italy): a combined geothermometric and isotopic ($\delta^{13}C$) perspective. J. Hydrol., 582, 124495. https://doi.org/10.1016/j.jhydrol.2019.124495.

Barbieri, M., Franchini, S., Barberio, M.D., Billi, A., Boschetti, T., Giansante, L., Gori, F., Jónsson, S., Petitta, M., Skelton, A., Stockmann, G., 2021. Changes in groundwater trace element concentrations before seismic and volcanic activities in Iceland during 2010-2018. Sci. Total Environ. 793, 14863. https://doi.org/10.1016/j.scitotenv.2021.148635.

Barchi, M.R., De Feyter, A., Magnani, M.B., Minelli, G., Pialli, G., Sotera, B.M., 1998a. The structural style of the Umbria-Marche fold and thrust belt. Mem. Soc. Geol. It., 52, 557–578.

Barchi, M., Landuzzi, A., Minelli, G., Pialli, G., 2001. Outer Northern Apennines. In: Vai, G. B., Martini, I. P., Anatomy of an orogen, the Apennines and adjacent Mediterranean Basins, 215-254, Kluwer Academic Publishers, Dordrecht.

Barchi, M., Minelli, G., Pialli, G., 1998b. The CROP 03 profile: a synthesis of results on deep structures of the Northern Apennines. Mem. Soc. Geol. It., 52, 383–400.

Barth, J.A.C., Cronin, A.A., Dunlop, J., Kalin, R.M., 2003. Influence of carbonates on the riverine carbon cycle in an anthropogenically dominated catchment basin: evidence from major elements and stable carbon isotopes in the Lagan River (N. Ireland). Appl. Geoch., 200 (3–4), 203–216. https://doi.org/10.1016/S0009-2541(03)00193-1.

Barth, S.R., 1993. Boron isotope variations in nature: a synthesis. Geol. Rundsch., 82, 640–651.

Barth, S.R., 2000. Geochemical and boron, oxygen and hydrogen isotopic constrains on the origin of salinity in groundwaters from the crystalline basement of the Alpine

Foreland. Appl. Geochem. 15, 937–952. https://doi.org/10.1016/S0883-2927(99)00101-8.
Berrettoni, C., Tolomeo, L., Veneri, F., 1986. Strontium isotopic composition and contents in gypsum from three Upper Miocene evaporitic basins of the Umbria-Marche-Romagna series (Italy). Per. Mineral., 55, 255–259.
Boncio, P., Brozzetti, F., Lavecchia, G., 2000. Architecture and seismotectonics of regional low-angle normal fault zone in Central Italy. Tectonics 19, 1038–1055. https://doi.org/10.1029/2000TC900023.
Boncio, P., Brozzetti, F., Ponziani, F., Barchi, M., Lavecchia, G., Pialli, G., 1998. Seismicity and extensional tectonics in the Northern Umbria-Marche Apennines. Mem. Soc. Geol. It., 52, 539–555.
Boni, C., 2010. Hydrogeological study for the identification, characterization and management of the groundwater resources in the Sibillini Mountains National Park (Central Italy). Italian Journal of Engineering Geology and Environment 2, 21–39.
Boni, C., Petitta, M., 2007. Hydrogeological study for the identification and characterization of aquifers recharging the springs of the perennial streams of the Sibillini Mountains, extended to the whole area of the National Park; Technical Note, Dipartimento di Scienze della Terra, Università "La Sapienza" di Roma, Autorità di Bacino del F. Parco Nazionale dei Monti Sibillini, Roma, Italy.
Boschetti, T., Barbieri, M., Barberio, M.D., Billi, A., Franchini, S., Petitta, M., 2019. CO_2 inflow and elements desorption prior to a seismic sequence, Amatrice-Norcia 2016, Italy. Geochem. Geophys. Geosyst. 20, 2303–2317.
Boschetti, T., Cortecci, G., Toscani, L., Iacumin, P., 2011. Sulfur and oxygen isotope compositions of Upper Triassic sulfates from Northern Apennines (Italy): paleogeographic and hydrogeochemical investigations. Geologia Acta 9 (2), 129–147. https://doi.org/10.1344/105.000001690.
Boschetti, T., Toscani, L., Iacumin, P., Selmo, E., 2017. Oxygen, hydrogen, boron and lithium isotope data of a natural spring water with an extreme composition: a fluid from the dehydrating slab? Aquat. Geochem. 23, 299–313. https://doi.org/10.1007/s10498-017-9323-9.
Boschetti, T., Toscani, L., Salvioli Mariani, E., 2015. Boron isotope geochemistry of Na-carbonate, Na-chloride, and Ca-chloride waters from the Northern Apennines foredeep basin: other pieces of the sedimentary basin puzzle. Geofluids 15, 546–562. https://doi.org/10.1111/gfl.12124.
Bottrell, S., Hipkins, E.V., Lane, J.M., Zegos, R.A., Banks, D., Frengstad, B.S., 2019. Carbon-13 in groundwater from English and Norwegian crystalline rock aquifers: a tool for deducing the origin of alkalinity? Sustain. Water Resour. Manag., 5, 267–287. https://doi.org/10.1007/s40899-017-0203-7.
Bowen, G.J., 2008. Spatial analysis of the intra-annual variation of precipitation isotoperatios and its climatological corollaries. J. Geophys. Res. 113. https://doi.org/10.1029/2007JD009295.
Bullen, T.D., Krabbenhoft, D.P., Kendall, C., 1996. Kinetic and mineralogical controls on the evolution of groundwater chemistry and $^{87}Sr/^{86}Sr$ in a sandy silicate aquifer, northern Wisconsin, USA. Geochim. Cosmochim. Acta 60, 1807–1821. https://doi.org/10.1016/0016-7037(96)00052-X.
Cambi, C., Mirabella, F., Petitta, M., Banzato, F., Beddini, G., Cardellini, C., Fronzi, D., Mastrorillo, L., Tazioli, A., Valigi, D., 2022. Reaction of the carbonate Sibillini Mountains Basal aquifer (Central Italy) to the extensional 2016-2017 seismic sequence. Sci. Rep. 12 (1), 22428. https://doi.org/10.1038/s41598-022-26681-2.
Capaccioni, B., Didero, M., Paletta, C., Salvadori, P., 2001. Hydrogeochemistry of groundwaters from carbonate formations with basal gypsiferous layers: an example from the Mt. Catria-Mt. Nerone ridge (Northern Apennines, Italy). J. Hydrol. 253, 14–26. https://doi.org/10.1016/S0022-1694(01)00480-2.
Capaccioni, B., Vaselli, O., Moretti, E., Tassi, F., Franchi, R., 2003. The origin of thermal waters from the eastern flank of the Dead Sea Rift Valley (western Jordan). Terra Nova 15, 145–154. https://doi.org/10.1046/j.1365-3121.2003.00476.x.
Capuano, N., 2009. Note illustrative della Carta Geologica d'Italia alla scala 1:50 000 "Foglio 279 – Urbino". Servizio Geologico d'Italia, Roma.
Capuano, N., Tonelli, G., Veneri, F., 1986. Ricostruzione dell'evoluzione paleogeografica del margine appennino nell'area feltresca (Marche settentrionali) durante il Pliocene Inferiore e Medio. Mem. Soc. Geol. It., 35, 163–170.
Castorina, F., Masi, U., 2011. Sr isotopes and Romagna wines: an opportunity for better trading? Environmental Quality 7, 41–48. https://doi.org/10.6092/issn.2281-4485/3832.
Centamore, E., Chiocchini, M., Deiana, G., Micarelli, A., Pieuriccini, U., 1971. Contributo alla conoscenza del Giurassico dell'Appennino umbro-marchigiano. Studi Geol. Camerti 1, 7–89.
Centamore, E., Deiana, G., Micarelli, A., Potetti, M., 1986. Il Trias-Paleogene delle Marche. Studi Geol. Camerti, Vol. Spec. "la Geologia Delle Marche" 7–27.
Centamore, E., Fumanti, F., Nisio, S., 2002. The Central-Northern Apennines geological evolution from Triassic to Neogene time. Boll. Soc. Geol. It. Special 1, 181–197.
Centamore, E., Micarelli, A., 1991. Stratigrafia. In: Minetti, A., Nanni, T., Perilli, F., Polonara, L., Principi, M. (Eds.), L'ambiente Fisico Delle Marche. Regione Marche, Assessorato Urbanistica e Ambiente, Ancona, pp. 5–58.
Cerling, T.E., Solomon, D.K., Quade, J., Bowman, J.R., 1991. On the isotopic composition of carbon in soil carbon dioxide. Geochim. Cosmochim. Acta 55, 3403–3405. https://doi.org/10.1016/0016-7037(91)90498-T.
Chemeri, L., Taussi, M., Cabassi, J., Capecchiacci, F., Randazzo, A., Tassi, F., Renzulli, R., Vaselli, O., 2024. Groundwater and dissolved gases geochemistry in the Pesaro-Urbino province (northern Marche, central Italy) as tool for seismic surveillance and sustainability. Sustainability 16, 5178. https://doi.org/10.3390/su16125178.
Chemeri, L., Taussi, M., Fronzi, D., Cabassi, J., Mazzoli, S., Tazioli, A., Renzulli, A., Vaselli, O., 2025. Groundwater hydrogeochemical changes predating and following the November 9, 2022 M_w 5.5 Adriatic Offshore earthquake. J. Hydrol., 653, 132792. https://doi.org/10.1016/j.jhydrol.2025.132792.
Chiodini, G., Cardellini, C., Di Luccio, F., Selva, J., Frondini, F., Caliro, S., Rosiello, A., Beddini, G., Ventura, G., 2020. Correlation between tectonic CO_2 earth degassing and seismicity is revealed by a 10-year record in the Apennines, Italy. Sci. Adv. 6 (35), eabc2938. https://doi.org/10.1126/sciadv.abc2938.
Chiodini, G., Frondini, F., Cardellini, C., Parello, F., Peruzzi, L., 2000. Rate of diffuse carbon dioxide degassing estimated from carbon balance of regional aquifers. The case of central Apennines, Italy. J. of Geophys. Res., 105, 8423–.
Cicerone, R.D., Ebel, J.E., Britton, J., 2009. A systematic compilation of earthquake precursors. Tectonophysics 476, 371–396. https://doi.org/10.1016/j.tecto.2009.06.008.
Claesson, L., Skelton, A., Graham, C., Dieti, C., Mörth, C.-M., Torssander, P., Kockum, I., 2004. Hydrogeochemical changes before and after a major earthquake. Geology 32, 641–644.
Claesson, L., Skelton, A., Graham, C., Mörth, C.-M., 2007. The timescale and mechanisms of fault sealing and water-rock interaction after an earthquake. Geofluids 7, 427–440. https://doi.org/10.1111/j.1468-8123.2007.00197.x.
Clark, I.D., 2015. Groundwater geochemistry and isotopes. CRC Press, Boca Raton, London, New York.
Clark, I.D., Fritz, F., 1997. Environmental isotopes in hydrogeology. Lewis Publishers, New York.
Conti, P., Cornamusini, G., Carmignani, L., 2020. An outline of the geology of the Northern Apennines (Italy), with geological map 1:250.000 scale. Ital. J. Geosci., 139, 149–194. https://doi.org/10.3301/IJG.2019.25.
Cortecci, G., Calafato, A., Boschetti, T., 1999. New chemical and isotopic data on the groundwater system of Bagno di Romagna, northern Apennines, Emilia-Romagna province. Italy. Miner. Petrog. Acta, XLII, pp. 89–101.
Cortecci, G., Dinelli, E., Bencini, A., Adorni Braccesi, A., La Ruffa, G., 2002. Natural and anthropogenic SO4 sources in the Arno River catchment, Northern Tuscany, Italy: a chemical and isotopic reconnaissance. Appl. Geochem., 17, 79–92. https://doi.org/10.1016/S0883-2927(01)00100-7.
Cortecci, G., Dinelli, E., Boschetti, T., 2007. The River Arno catchment, northern Tuscany: chemistry of waters and sediments from the River Elsa and River Era sub-basins, and sulphur and oxygen isotopes of aqueous sulphate. Hydrol. Process. 21, 1–20. https://doi.org/10.1002/hyp.6270.
Cortecci, G., Reyes, E., Berti, G., Casati, P., 1981. Sulfur and oxygen isotopes in italian marine sulfates of Permian and Triassic Ages. Chem. Geol., 34, 65–79.
Cresta, S., Monechi, S., Parisi, G., 1989. Mesozoic-Cenozoic stratigraphy in the Umbria-Marche area. Memorie Descrittive della Carta Geologica d'Italia, 39, Serv. Geologico d'Italia, Roma.
D'Antonio, L., Fronzi, D., Mammoliti, E., Palpacelli, S., Ianni, C., Tonelli, M., Tazioli, A., 2024. Hydraulic conductivity estimation through the use of tracers tests and geomechanical survey: preliminary outcomes from the Montagna dei Fiori carbonate aquifer (Central Italy). Italian Journal of Engineering Geology and Environment, (special Issue 1), 85–93. https://doi.org/10.4408/IJEGE.2024-01.S-10.
De Donatis, M., Alberti, M., Cipicchia, M., Munoz-Guerrero, N., Pappafico, G.F., Susini, S., 2020. Workflow of digital field mapping and drone-aided survey for the identification and characterization of capable faults: the case of normal fault system in the Mt. Nerone area (Northern Apennines, Italy). Int. J. Geo-Inf., 9, 616. https://doi.org/10.3390/ijgi9110616.
Deutsch, W.J., 2020. Groundwater geochemistry: fundamentals and applications to contamination. CRC Press.
DISS Working Group, 2021. Database of Individual Seismogenic Sources (DISS), Version 3.3.0: a compilation of potential sources for earthquakes than M 5.5 in Italy and surrounding areas. Istituto Nazionale Di Geofisica e Vulcanologia (INGV).
Doglioni, C., Barba, S., Carminati, E., Riguzzi, F., 2014. Fault on-off versus coseismic fluid reactions. Geosci. Front. 5 (6), 767–780. https://doi.org/10.1016/j.gsf.2013.08.004.
Dotsika, E., Poutoukis, D., Kloppmann, W., Guerrot, C., Voutsa, D., Kouimtzis, T.H., 2010. The use of O, H, B, Sr and S isotopes for tracing the origin of dissolved boron in groundwater in Central Macedonia. Greece. Appl. Geochem., 25, 1783–1796. https://doi.org/10.1016/j.apgeochem.2010.09.006.
Farina, D., Bisiccia, C., Severini, A., 2012. Hydrogeology of the "Maiolica" and "Scaglia" carbonatic aquifers in the northeastern flank of the Mt. Paganuccio (Furlo Mountains, Marche, Italy). Flowpath – Percorsi di Idrogeologia, Bologna, 20-22 June 2012.
Farina, D., Cavitolo, P., 2016. Climate and land use changes as origin of the water cycle variations and sediment transport in Pesaro Urbino Province, Central and Eastern Italy. Acque Sotterranee-Italian Journal of. Groundwater 5 (3). https://doi.org/10.7343/as-2016-207.
Feng, X., Faiia, A. M., Posmentier, 2012. Seasonality of isotopes in precipitation: A global perspective. Journal of Geophysical Research, 114, https://doi.org/10.1029/2008JD011279.
Franchini, F., Agostini, S., Barberio, M.D., Barbieri, M., Billi, A., Boschetti, T., Pennisi, M., Petitta, M., 2021. HydroQuakes, central Apennines: towards a hydrogeochemical monitoring network for seismic precursors and the hydro-seismo-sensitivity of boron. J. Hydrol. 598, 125754. https://doi.org/10.1016/j.jhydrol.2020.125754.
Frei, R., Frei, K.M., Kristiansen, S.M., Jessen, S., Schullehner, J., Hansen, B., 2020. The link between surface water and groundwater-based drinking water – strontium isotope spatial distribution patterns and their relationships to Danish sediments. Appl. Geochem. 121, 104698. https://doi.org/10.1016/j.apgeochem.2020.104698.
Frondini, F., 2008. Geochemistry of regional aquifers systems hosted by carbonate-evaporite formations in Umbria and Southern Tuscany (central Italy). Appl. Geochem. 23, 2091–2104. https://doi.org/10.1016/j.apgeochem.2008.05.001.
Fronzi, D., Di Curzio, D., Rusi, S., Valigi, D., Tazioli, A., 2020. Comparison between periodic tracer tests and time-series analysis to assess mid- and long-term recharge

model changes due to multiple strong seismic events in carbonate aquifers. Water 12 (11), 3073. https://doi.org/10.3390/w12113073.
Fronzi, D., Mirabella, F., Cardellini, C., Caliro, S., Palpacelli, S., Cambi, C., Valigi, D., Tazioli, D., 2021. The role of faults in groundwater circulation before and after seismic events: insights from tracers, water isotopes and geochemistry. Water 13 (11), 1499. https://doi.org/10.3390/w13111499.
Fronzi, D., Gaiolini, M., Mammoliti, E., Colombani, N., Palpacelli, S., Marcellini, M., Tazioli, A., 2022. Groundwater-surface water interaction revealed by meteorological trends and groundwater fluctuations on stream water level. Acque Sotterranee-Italian Journal of Groundwater 11 (2), 19–28. https://doi.org/10.7343/as-2022-574.
Fronzi, D., Cambi, C., Fiorucci, F. M., Liso, L. S., Manucci, A., Mazzocca, M., Mirabella, F., Parise, M., Tazioli, A., Valigi, D., 2024a, Updating of traditional groundwater budget and recharge assessment by using the APLIS method for the karst Scirca spring (Central Italy). In Print. Eurokarst, 2024. Conference proceedings. Springer.
Gallerini, G., De Donatis, M., 2009. 3D modeling using geognostic data: the case of the low valley of the Foglia river (Italy). Computer & Geosciences 35 (1), 146–164. https://doi.org/10.1016/j.cageo.2007.09.012.
Gori, F., Barberio, M.D., 2022. Hydrogeochemical changes before and during the 2019 Benevento seismic swarm in central-southern Italy. J. Hydrol. 604, 127250. https://doi.org/10.1016/j.jhydrol.2021.127250.
Gori, F., Paternoster, M., Barbieri, M., Buttitta, D., Caracausi, A., Parente, F., Sulli, A., Petitta, M., 2023. Hydrogeochemical multi-component approach to assess fluids upwelling and mixing in shallow carbonate-evaporitic aquifers (Contursi area, southern Apennines, Italy). J. Hydrol., 619, 129258. https://doi.org/10.1016/j.jhydrol.2023.129258.
Grassa, F., Capasso, G., Favara, R., Inguaggiato, S., 2006. Chemical and isotopic composition of waters and dissolved gases in some thermal springs of Sicily and adjacent Volcanic Island. Italy. Pure and Applied Geophysics 163 (4), 781–807. https://doi.org/10.1007/s00024-006-0043-0.
Guan, H., Simmons, C. T., Love, A., J., 2009. Orographic controls on rain water isotope distribution in the Mount Lofty Ranges of South Australia. Journal of Hydrology, 374, 255-264. https://doi.org/10.1016/j.jhydrol.2009.06.018.
Guerrot, C., Millot, R., Robert, M., Négrel, P., 2011. Accurate and high-precision determination of boron isotopic ratios at low concentration by MC-ICP-MS (Neptune). Geostand. Geoanal. Res. 35, 275–284. https://doi.org/10.1111/j.1751-908X.2010.00073.x.
Hasenmueller, E.A., Criss, R.E., 2013. Multiple sources of boron in urban surface waters and groundwaters. Sci. Total Environment 447, 235–247. https://doi.org/10.1016/j.scitotenv.2013.01.001.
Hao, S., Li, F., Li, Y., Gu, C., Zhang, Q., Qiao, Y., Jiao, L., Zhu, N., 2019. Stable isotope evidence for identifying the recharge mechanisms of precipitation, surface water, and groundwater in the Ebinur Lake basin. Sci. Total Environ. 657, 1041–1050. https://doi.org/10.1016/j.scitotenv.2018.12.102.
Holser, W.T., Kaplan, I.R., 1966. Isotope geochemistry of sedimentary sulfates. Chem. Geol., 1, 93–135. https://doi.org/10.1016/0009-2541(66)90011-8.
Hosono, T., Masaki, Y., 2020. Post-seismic hydrochemical changes in regional groundwater flow systems in response to the 2016 M_w 7.0 Kumamoto earthquake. J. Hydrol. 580, 124340. https://doi.org/10.1016/j.jhydrol.2019.124340.
Hosono, T., Yamada, C., Manga, M., Wang, C.-Y., Tanimizu, M., 2020. Stable isotopes show that earthquakes enhance permeability and release water from mountains. Nat. Commun. 11, 1–9. https://doi.org/10.1038/s41467-020-16604-y.
Hosono, T., Yamada, C., Shibata, T., Tawara, Y., Wang, C.-Y., Manga, M., Rahman, A.T. M.S., Shimada, J., 2019. Coseismic groundwater drawdown along crustal ruptures during the 2016 M_w 7.0 Kumamoto earthquake. Water Resource Research 55, 5891–5903. https://doi.org/10.1029/2019WR024871.
Knöller, K., Vogt, C., Feisthauer, S., Weise, S.M., Weiss, H., Richnow, H.-H., 2008. Sulfur cycling and biodegradation in contaminated aquifers: insights from stable isotopes investigations. Environ. Sci. Technol., 42 (21), 7807–7812. https://doi.org/10.1021/es800331p.
Jørgensen, N.O., Andersen, M.S., Engesgaard, P., 2008. Investigations of a dynamic seawater intrusion event using strontium isotopes ($^{87}Sr/^{86}Sr$). J. Hydrol., 348, 257–269. https://doi.org/10.1016/j.jhydrol.2007.10.001.
Langelier, W.F., Ludwig, H.F., 1942. Graphical methods for indicating the mineral character of natural waters. Journal (american Water Works Association) 34 (3), 335–352.
Lavecchia, G., Boncio, P., Creati, N., 2003. A lithospheric-scale seismogenic thrust in Central Italy. J. Geodyn., 36, 79–94. https://doi.org/10.1016/S0264-3707(03)00040-1.
Lavecchia, G., Barchi, M., Brozzetti, F., Menichetti, M., 1994. Sismicità e tettonica nell'area umbro-marchigiana. Boll. Soc. Geol. It., 113, 483–500.
Lee, H.A., Hamm, S.-Y., Woo, N.C., 2017. Groundwater monitoring network for earthquake surveillance and prediction. Economic and Environmental Geology 50, 401–414.
Lee, H.A., Hamm, S.-Y., Woo, N.C., 2021. Pilot-scale groundwater monitoring network for earthquake surveillance and forecasting research in Korea. Water 13, 2448. https://doi.org/10.3390/w13172448.
Leeman, W. P., Sisson, V. B., 1996. Geochemistry of boron and its implications for crustal and mantle processes. In: Grew, E. S., Anovitz, L. M., (Eds), Boron: mineralogy, petrology and geochemistry, Review in Mineralogy, 33, 645-707.
Longinelli, A., Selmo, E., 2003. Isotopic composition of precipitation in Italy: a first overall map. J. Hydrol., 270, 75–88. https://doi.org/10.1016/S0022-1694(02)00281-0.
Lugli S., Bassetti M.A., Manzi V., Barbieri M., Longinelli A., Roveri M., 2007. The Messinian 'Vena del Gesso' evaporites revisited: characterization of isotopic composition and organic matter. In: Schreiber, B. C., Lugli, S. & Babel, M. (eds): Evaporites Through Space and Time. Geological Society, London, Special Publications, 285, 179–190. DOI: 10.1144/SP285.11. The Geological Society of London 2007.
Lundblad, S.P., 2019. Model for development of small carbonate platforms in the Umbria-Marche Apennines supported by strontium isotope stratigraphy. The Geological Society of America, Special Paper 542, 69–85. https://doi.org/10.1130/2019.2542(03).
MacNamara, J., Thode, H.G., 1950. Comparison of the isotope composition of terrestrial and meteoric sulfur. Phys. Rev., 78, 307–308.
Maesano, F. E., Buttinelli, M., Maffucci, R., Toscani, G., Basili, R., Bonini, L., Burrato, P., Fedorik, J., Fracassi, U., Panara, Y., Tarabusi, G., Tiberti, M. M., Valensise, G., Vallone, R., Vannoli, P., 2023. Buried alive: imaging of the 9 November 2022, M_2 5.5 earthquake source on the Offshore Adriatic blind thrust front of the Northern Apennines (Italy). Geophysical Research Letters, 50, e2022GL102299.
Mammoliti, E., Fronzi, D., Cambi, C., Mirabella, F., Cardellini, C., Paracchiola, E., Tazioli, A., Caliro, S., Valigi, D., 2022. A holistic approach to study groundwater-surface water modifications induced by strong earthquakes: the case of the Campiano catchment (Central Italy). Hydrology 9 (6), 97. https://doi.org/10.3390/hydrology9060097.
Mammoliti, E., Fronzi, D., Palpacelli, S., Biagiola, N., Tazioli, A., 2023. Assessment of urban landslide groundwater characteristics and origin using artificial tracers, hydro-chemical and stable isotope approaches. Environ. Earth Sci. 82 (9), 211. https://doi.org/10.1007/s12665-023-10887-2.
Mantovani, E., Viti, M., Babbucci, D., Tamburelli, C., Vannucchi, A., Falciani, F., Cenni, N., 2014. Assetto tettonico e potenzialità sismogenetica dell'Appennino Tosco-Umbro-Marchigiano. Università di Siena, Siena, Italy.
Martinis, B., Pieri, M., 1964. Alcune notizie sulla formazione evaporitica del Triassico superiore nell'Italia centrale e meridionale. Mem. Soc. Geol. It., 4 (1), 649–678.
Mastrorillo, L., Petitta, M., 2014. Hydrogeological conceptual model of the upper Chienti River basin aquifers (Umbria-Marche Apennines). Ital. J. Geosci. 133 (3), 396–408. https://doi.org/10.3301/IJG.2014.12.
Mastrorillo, L., Baldoni, T., Banzato, F., Boscherini, A., Cascone, D., Checcucci, R., Petitta, M., Boni, C., 2009. Quantitative hydrogeologicalanalysis of the carbonate domain of the Umbria region (central Italy). Ital. J. Eng. Geol. Environ. 1.
Mazzoli, S., Machiavelli, C., Ascione, A., 2014. The 2013 Marche off-shore earthquakes: new insights into the active tectonic setting of the outer-northern Apennines. J. Geol. Soc., 171, 457–460. https://doi.org/10.1144/jgs2013-091.
Mazzoli, S., Pierantoni, P.P., Borraccini, F., Paltrinieri, W., Deiana, G., 2005. Geometry, segmentation pattern and displacement variations along a major Apennine thrust zone, central Italy. J. Struct. Geol., 27, 1940–1953. https://doi.org/10.1016/j.jsg.2005.06.002.
Mazzoli, S., Santini, S., Macchiavelli, C., Ascione, A., 2015. Active tectonics of the outer Northern Apennines: Adriatic vs. Po Plain Seismicity. J. Geodynamics 84, 62–76. https://doi.org/10.1016/j.jog.2014.10.002.
Menichetti, M., Chirenco, M. I., Onac, B., Bottrell, S., 2017. Depositi di gesso nelle grotte del Monto Cucco e della Gola di Frasassi – Considerazione sulla speleogenesi. Atti del XX Congresso Nazionale di Speleologia, Iglesias 27-30 Aprile 2007, Memorie dell'Istituto Italiano di Speleologia, s.II, vol. XXI.
Merritt, D.A., Hayes, J.M., Des Marais, D.J., 1995. Carbon isotopic analysis of atmospheric methane by isotope-ratio-monitoring gas chromatography-mass spectrometry. Journal Geophysical Research 100D1, 1317–1326. https://doi.org/10.1029/94JD02689.
Meybeck, M., 1987. Global chemical weathering of surficial rocks estimated from river dissolved loads. Am. J. Sci., 287, 401–428. https://doi.org/10.2475/ajs.287.5.401.
Meyer, L., Menichetti, M., Nesci, O., Savelli, D., 2003. Morphotectonic approach to the drainage analysis in the North Marche region, central Italy. Quat. Int., 101–102, 157–167. https://doi.org/10.1016/S1040-6182(02)00098-8.
Minissale, A., Vaselli, O., 2011. Karst spring as "natural" pluviometers: constraints on the isotopic composition of rainfall in the Apennines of central Italy. Appl. Geochem. 26 (5), 838–852. https://doi.org/10.1016/j.apgeochem.2011.02.005.
Montegrossi, G., Tassi, F., Vaselli, O., Bidini, E., Minissale, A., 2006. A new, rapid and reliable method for the determination of reduced sulfur (S^{2-}) species in natural water discharges. Appl. Geochem. 21 (5), 849–857. https://doi.org/10.1016/j.apgeochem.2006.02.007.
Nanni, T., Vivalda, P., 2005. The aquifers of the Umbria-Marche Adriatic region: relationships between structural setting and groundwater chemistry. Boll. Soc. Geol. It., 124, 523–542.
Nanni, T., Vivalda, P.M., Palpacelli, S., Marcellini, M., Tazioli, A., 2020. Groundwater circulation and earthquake-related changes in hydrogeological karst environments: a case study of the Sibillini Mountains (central Italy) involving artificial tracers. Hydrgeol. J. 28 (7), 2409–2428. https://doi.org/10.1007/s10040-020-02207-w.
Nesci, O., Savelli, D., Troiani, F., 2008. Evoluzione tardo quaternaria dell'area di foce del Fiume Metauro (Marche Settentrionali). In: Collana dell'Autorità di Bacino della Basilicata, Proceedings of the "Coste: Prevenire, Programmare, Pianificare Conference", Maratea, Italy, 15-17 May 2008, Autorità di Bacino della Basilicata: Potenza, Italy, 9, 443-451.
Nisi, B., Buccianti, A., Vaselli, O., Perini, G., Tassi, F., Minissale, A., Montegrossi, G., 2008. Hydrogeochemistry and strontium isotopes in the Arno River Basin (Tuscany, Italy): constraints on natural controls by statistical models. J. Hydrol. 360, 166–183. https://doi.org/10.1016/j.jhydrol.2008.07.030.
Nisi, B., Raco, B., Dotsika, E., 2014. Groundwater contamination studies by environmental isotopes; a review. In: AA. VV. (Eds.), Environment, Energy and Climate Change I: Environmental Chemistry of Pollutants and Wastes. Springer-Verlag Berlin Heidelberg.
Nisi, B., Vaselli, O., Taussi, M., Doveri, M., Menichini, M., Cabassi, J., Raco, B., Botteghi, S., Mussi, M., Masetti, G., 2022. Hydrogeochemical surveys of shallow

coastal aquifers: a conceptual model to set-up a monitoring network and increase the resilience of a strategic groundwater system to climate change and anthropogenic pressure. Appl. Geoch., 142, 105305. https://doi.org/10.1016/j.apgeochem.2022.105350.

North, J.C., Frew, R.D., Peake, B.M., 2003. The use of carbon and nitrogen isotope ratios to identify landfill leachate contamination: Green Island Landfill, Dunedin. New Zealand. Environ. International 30, 631–637. https://doi.org/10.1016/j.envint.2003.12.006.

Papaslioti, E.-M., Pérez-López, R., Parviainen, A., Sarmiento, A.M., Nieto, J.M., Marchesi, C., Delgado Huertas, A., Garrido, J.C., 2018. Effects of seawater mixing on the mobility of trace elements in acid phosphogypsum leachates. Marine Pollution Bullettin 127, 695–703. https://doi.org/10.1016/j.marpolbul.2018.01.001.

Pawellek, F., Frauenstein, F., Veizer, J., 2002. Hydrogeochemistry and isotope chemistry of the upper Danube River. Geochem. Cosmoch. Acta 66 (21), 3839–3853. https://doi.org/10.1016/S0016-7037(01)00880-8.

Pauselli, C., Gola, G., Mancinelli, P., Trumpy, E., Saccone, M., Manzella, A., Ranalli, G., 2019. A new surface heat flow map of the Northern Apennines between latitudes 42.5 and 44.5 N. Geothermics 81, 39–52. https://doi.org/10.1016/j.geothermics.2019.04.002.

Pennisi, M., Gonfiantini, R., Grassi, S., Squarci, P., 2006. The utilization of boron and strontium isotopes for the assessment of boron contamination of the Cecina River alluvial aquifer (central-western Tuscany, Italy). Appl. Geochem. 21, 643–655. https://doi.org/10.1016/j.apgeochem.2005.11.005.

Petitta, M., Scarascia Mugnozza, G., Barbieri, M., Bianchi Fasani, G., Esposito, C., 2010. Hydrodynamic and isotopic investigations for evaluating the mechanisms and amount of groundwater seepage through a rockslide dam. Hydrol. Process. 24, 3510–3520.

Pezzo, G., Billi, A., Carminati, E., De Gori, P., Devoti, R., Lucente, F.P., Palano, M., Petracchini, L., Serpelloni, E., Tavani, S., Chiarabba, C., 2023. Seismic source of identification of the 9 November 2022 M_w 5.5 offshore Adriatic Sea (Italy) earthquake from GNSS data and aftershock relocation. Sci. Rep. 13, 11474. https://doi.org/10.1038/s41598-023-38150-5.

Pierantoni, P.P., Chicco, J., Costa, M., Invernizzi, C., 2019. Plio-Quaternary transpressive tectonics: a key factor in the structural evolution of the outer Apennine-Adriatic system. Italy. J. Geol. Soc., 176 (6), 1273–1283. https://doi.org/10.1144/jgs2018-199.

Puig, R., Soler, A., Widory, D., Mas-Pla, J., Domènech, C., Otero, N., 2017. Characterizing sources and natural attenuation of nitrate contamination in the Baix Ter aquifer system (NE Spain) using a multi-isotope approach. Sci. Total Environ. 580, 518–532. https://doi.org/10.1016/j.scitotenv.2016.11.206.

Reddy, D.V., Kumar, D., Rao, P.N., 2017. Long-term hydrogeochemical earthquake precursors studies at Konya-Warna reservoir in Western India. J. Geol. Soc. India 90, 720–727. https://doi.org/10.1007/s12594-017-0781-x.

Renzulli, A., Upton, B.G.I., Boyce, A., Ellam, R.B., 1998. Petrology of quartz syenite and hauyne syenite clasts from the Pitigliano Formation, Latera caldera, Vulsini District. Central Italy. European Journal of Mineralogy 10 (2), 333–354. https://doi.org/10.1127/ejm/10/2/0333.

Ricci Lucchi, F., 1986. The Oligocene to recent foreland basins of the Northern Apennines. In: Allen, P. A., Homewood, P., (Eds.), Foreland Basins. International Association of Sedimentologists. Special Publications, 8, 105-139. Blackwell Scientific Publications, Oxford.

Salata, G.G., Roelke, L.A., Cifuentes, L.A., 2000. A rapid and precise method for measuring stable isotope ratios of dissolved inorganic carbon. Mar. Chem., 69, 153–161. https://doi.org/10.1016/S0304-4203(99)00102-4.

Santantonio, M., 1993. Facies associations and evolution of pelagic carbonate platform/basin systems: examples from the Italian Jurassic. Sedimentology 40 (6), 1039–1067. https://doi.org/10.1111/j.1365-3091.1993.tb01379.x.

Semhi, K., Abdalla, O., Al Abri, R., Al Hasni, T., Clark, I.D., 2017. Strontium isotopes as a tool for estimation of groundwater recharge and aquifer connectivity. Groundwater for a Sustainable Development 4, 1–11. https://doi.org/10.1016/j.gsd.2016.11.001.

Skelton, A., Andrén, M., Kristmannsdóttir, H., Stockmann, G., Mörth, C.-M., Sveinbjörnsdòttir, A., Jónsson, S., Sturkell, E., Guorúnardóttir, H.-R., Hjartarson, H., Siegmund, H., Kockum, I., 2014. Changes in groundwater chemistry before two consecutive earthquakes in Iceland. Nat. Geosci. 7, 752–756. https://doi.org/10.1038/ngeo2250.

Skelton, A., Claesson, L., Wästeby, N., Andrén, M., Stockmann, G., Sturkell, E., Mörth, C.-M., Stefansson, A., Tollefsen, E., Siegmund, H., Keller, N., Kjartansdóttir, R., Hjartarson, H., Kockum, I., 2019. Hydrochemical changes before and after earthquakes based on long-term measurements of multiple parameters at two sites in Northern Iceland - a review. J. Geophys. Res. Solid Earth 124, 2702–2720. https://doi.org/10.1029/2018JB016757.

Skelton, A., Sturkell, E., Mörth, C.-M., Stockmann, G., Jónsson, S., Stefansson, A., Liljedahl-Claesson, L., Wästeby, N., Andrén, M., Tollefsen, E., Robin, J.G., Keller, N., Geirsson, H., Hjartarson, H., Kockum, I., 2024. Towards a method for forecasting earthquakes in Iceland using changes in groundwater chemistry. Commun. Earth Environ., 5, 662. https://doi.org/10.1038/s43247-024-01852-3.

Smeraglia, L., Bernasconi, S.M., Berra, F., Billi, A., Boschi, C., Caracausi, A., Cariminati, E., Castorina, F., Doglioni, C., Italiano, F., Rizzo, A.L., Uysal, I.T., Zhao, J.X., 2018. Crustal-scale fluid circulation and co-seismic shallow comb-veining along the longest normal fault of the central Apennines. Italy. Earth Planet. Sci. Lett., 498, 152–168. https://doi.org/10.1016/j.epsl.2018.06.013.

Spivack, A.J., Edmond, J.M., 1987. Boron isotope exchange between seawater and the oceanic crust. Geochim. Cosmochim. Acta 51 (5), 1033–1043. https://doi.org/10.1016/0016-7037(87)90198-0.

Szaran, J., Niezgoda, H., Halas, S., 1998. New determinations of oxygen and sulfur isotope fractioning between gypsum and dissolved sulphate. RMZ Mater. Geoenviron., 45, 180–182.

Tamburini, A., Betti, M., Arvanitis, S.D., Giannotti, P., Giordani, M., Magnoni, M., Sacchi, E.M., 2017. Il bacino sulfureo dell'Urbinate (Appennino Marchigiano esterno). OPERA IPOGEA 1–2, 69–77.

Tamburini, A., Menichetti, M., 2020. Groundwater circulation in fractured and karstic aquifers of the Umbria-Marche Apennine. Water 12 (4), 1039. https://doi.org/10.3390/w12041039.

Tassi, F., Garofalo, P.S., Turchetti, F., De Santis, D., Capecchiacci, F., Vaselli, O., Cabassi, J., Venturi, S., Vannini, S., 2022. Insights into the Porretta Terme (northern Apennines, Italy) hydrothermal system revealed by geochemical data on presently discharging thermal waters and paleofluids. Environ. Geochem. Health 44, 1925–1948. https://doi.org/10.1007/s10653-020-00762-5.

Taussi, M., Borghi, W., Gliaschera, M., Renzulli, A., 2021. Defining the shallow geothermal heat-exchange potential for a lower fluvial plain of the central Apennines: the Metauro Valley (Marche region, Italy). Energies 14, 768. https://doi.org/10.3390/en14030768.

Taussi, M., Gozzi, C., Vaselli, O., Cabassi, J., Menichini, M., Doveri, M., Romei, M., Ferretti, A., Gambioli, A., Nisi, B., 2022. Contamination assessment and temporal evolution of nitrates in the shallow aquifer of the Metauro River Plain (Adriatic Sea, Italy) after remediation actions. Int. J. Environ. Res. Public Health 19, 12231. https://doi.org/10.3390/ijerph191912231.

Taussi, M., Vespasiano, G., Chemeri, L., Bonì, R., Nisi, B., Vaselli, O., Delgado-Huertas, A., Apollaro, C., Tardani, D., Farina, D., Renzulli, A., 2024. Assessing anthropogenic and natural influences on water quality in a critical shallow groundwater system: insights from the Metauro River basin (Central Italy). Groundwater for a Sustainable Development 27, 101361. https://doi.org/10.1016/j.gsd.2024.101361.

Tavernelli, E., 1997. Structural evolution of a foreland fold-and-thrust belt: the Umbria-Marche Apennines. Italy. J. Struct. Geol., 19 (3–4), 523–534. https://doi.org/10.1016/S0191-8141(96)00093-4.

Tazioli, A., Fronzi, D., Palpacelli, S., 2024. Regional vs. local isotopic gradient: insights and modelling from mid-mountain areas in Central Italy. Groundwater. https://doi.org/10.1111/gwat.13395.

Teloni, S., Valente, E., Ascione, A., Mazzoli, S., Perantoni, P.P., Invernizzi, M.C., 2024. Morphostructural evidence of crustal-scale, active along-strike segmentation of the Umbria-Marche Apennines. Italy. Tectonophysics 891, 230527. https://doi.org/10.1016/j.tecto.2024.230527.

Thode, H.G., 1991. Sulphur isotopes in nature and in the environment: an overview. In: Krouse, H.R., Grinenko, V.A. (Eds.), Stable Isotopes: Natural and Anthropogenic Sulphur in the Environment. Wiley.

Thomas, D., 1988. Geochemical precursors to seismic activity. Pure Appl. Geophys., 126, 241–266. https://doi.org/10.1007/BF00878998.

Toscani, L., Venturelli, G., Boschetti, T., 2001. Sulphide-bearing waters in Northern Apennines, Italy: general features and water-rock interaction. Appl. Geochem. 7, 195–216. https://doi.org/10.1023/A:1012941328028.

Valigi, D., Fronzi, D., Cambi, C., Beddini, G., Cardellini, C., Checcucci, R., Mastrorillo, L., Mirabella, F., Tazioli, A., 2020. Earthquake-induced spring discharge modifications: the Pescara di Arquata spring reaction to the August-October 2016 Central Italy earthquakes. Water 12 (3), 767. https://doi.org/10.3390/w12030767.

Valigi, D., Cambi, C., Checcucci, R., Di Matteo, L., 2021. Transmissivity estimates by specific capacity data of some fractured Italian carbonate aquifers. Water 13 (10), 1374. https://doi.org/10.3390/w13101374.

Venturelli, G., Boschetti, T., Duchi, V., 2003. Na-carbonate waters of extreme composition: possible origin and evolution. Geochem. J. 37 (3), 351–366. https://doi.org/10.2343/geochemj.37.351.

Venturelli, G., Toscani, L., Mucchino, C., Voltolini, C., 2000. Study of water-rock interaction of spring waters in the north-Apennines. Anal. Chim. 90, 359–368.

Venturi, S., Tassi, F., Bicocchi, G., Cabassi, J., Capecchiacci, F., Capasso, G., Vaselli, O., Ricci, A., Grassa, F., 2017. Fractionation processes affecting the stable carbon isotope signature of thermal waters from hydrothermal/volcanic systems: the examples of Campi Flegrei and Vulcano Island (southern Italy). J. Volcanol. Geoth. Res. 345, 46–57. https://doi.org/10.1016/j.jvolgeores.2017.08.001.

Vergni, L., Di Lena, B., Chiaudani, A., 2016. Statistical characterisation of winter precipitation in the Abruzzo region (Italy) in relation to the North Atlantic Oscillation (NAO). Atmos. Res. 178–179, 279–290. https://doi.org/10.1016/j.atmosres.2016.03.028.

Verma, M.P., van Geldern, R., Carvalho, M.C., Grassa, F., Delgado-Huertas, A., Monvoisin, G., Carrizo, D., 2020. Interlaboratory test for stable carbon isotope analysis of dissolved inorganic carbon in geothermal fluids. Rapid Commun. Mass Spectrom. 34, e8685.

Vespasiano, G., Cianflone, G., Marini, L., De Rosa, R., Polemio, D., Walraevens, K., Vaselli, O., Pizzino, L., Cinti, D., Capecchiacci, F., Barca, D., Dominici, R., Apollaro, C., 2023. Hydrogeochemical and isotopic characterization of the Gioia Tauro coastal plain (Calabria – Southern Italy): a multidisciplinary approach for a focused management of vulnerable strategic systems. Sci. Total Environ. 862, 160694. https://doi.org/10.1016/j.scitotenv.2022.160694.

Vespasiano, G., Marini, L., Muto, F., Aiuqué, L.F., Cipriani, M., De Rosa, R., Critelli, S., Gimeno, M.J., Blasco, M., Dotsika, E., Apollaro, C., 2021. Chemical isotopic and geotectonic relations of the warm and cold waters of the Cotronei (Ponte Coniglio), Bruciarello and Repole thermal waters (Calabria-Southern Italy). Geothermics 96, 102228. https://doi.org/10.1016/j.geothermics.2021.102228.

Viaroli, S., Mirabella, F., Mastrorillo, L., Angelini, S., Valigi, D., 2021. Fractured carbonate aquifers of Sibillini Mts. (Central Italy). Journal of Maps, 17:2, 140–149, https://doi.org/10.1080/17445647.2021.1894252.

VIDEPI, 2009. Visibilità dei Dati afferenti all'attività di Esplorazione Petrolifera in Italia (Visibility of Data relating to Oil Exploration Activity in Italy). Available online at https://www.videpi.com/videpi/videpi.asp.

Wang, C.H., Wang, C.-Y., Kuo, C.-H., Chen, W.-F., 2005. Some isotopic and hydrological changes associated with the 1999 Chi-Chi earthquake. Taiwan. the Island Arc 14 (1), 37–54.

Wang, C.-Y., Manga, M., 2021. Water and earthquakes. Springer Nature.

Xu, Y., Liu, W., Xu, B., Xu, Z., 2024. Riverine sulfate sources and behaviors in arid environment, Northwest China: constraints from sulfur and oxygen isotopes. J. Environmental Sciences 137, 716–731. https://doi.org/10.1016/j.jes.2023.03.024.

Yang, Q., Mu, H., Guo, J., Bao, X., Martin, D., 2019. Temperature and rainfall amount effects on hydrogen and oxygen stable isotope in precipitation. Quat. Int. 519, 25–31. https://doi.org/10.1016/j.quaint.2019.01.027.

Zhang, D., Xue, T., Xiao, J., Chai, N., Gong, S., 2024. Significant influence of water diversion and anthropogenic input on riverine sulfate based on sulfur and oxygen isotopes. J. Hazardous Materials 461, 132622. https://doi.org/10.1016/j.jhazmat.2023.132622.